X-660-73-315
PREPRINT

NASA TM X- 70507

GODDARD CONTRIBUTIONS TO THE LOS ALAMOS CONFERENCE ON TRANSIENT COSMIC GAMMA- AND X-RAY SOURCES

LOS ALAMOS, NEW MEXICO
SEPTEMBER 20 AND 21, 1973

OCTOBER 1973

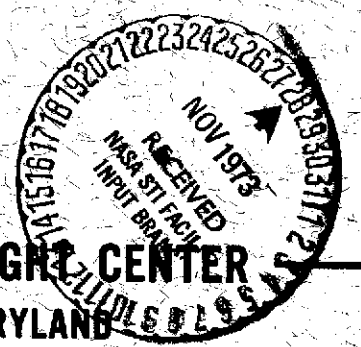

GODDARD SPACE FLIGHT CENTER
GREENBELT, MARYLAND

(NASA-TM-X-70507) GODDARD CONTRIBUTIONS TO THE LOS ALAMOS CONFERENCE ON TRANSIENT COSMIC GAMMA AND X-RAY SOURCES (NASA) ~~101~~ 91 p HC $7.25 CSCL 03B

N74-11609 THRU N74-11616
Unclas
G3/29 21596

GODDARD CONTRIBUTIONS TO THE LOS ALAMOS CONFERENCE ON TRANSIENT COSMIC GAMMA- AND X-RAY SOURCES

(Los Alamos, New Mexico, September 20 and 21, 1973)

OCTOBER 1973

TABLE OF CONTENTS*

*In order of presentation at the Conference.

N74-11610

IMP-6 OBSERVATIONS OF THE ENERGY SPECTRA OF COSMIC GAMMA-RAY BURSTS*

T. L. Cline and U. D. Desai
NASA/Goddard Space Flight Center
Greenbelt, Maryland 20771

A talk presented at the Los Alamos Conference on Transient Cosmic Gamma- and X-Ray Sources, September 20, 1973, delivered by U. D. Desai.

INTRODUCTION

The occurrence of intense, short bursts of 0.1 to 1.2-MeV cosmic gamma rays, recently found using multiple Vela satellites (Klebesadel et al., 1973), has been confirmed with measurements from the IMP-6 satellite. Observations regarding times of occurrence, photon flux, and temporal and spectral characteristics of the bursts are entirely consistent. In particular, since the IMP-6 instrument incorporates a hard X-ray detector with active particle rejection and full-time omnidirectional particle intensity monitoring, the results fully confirm and establish the hard X-ray or gamma-ray nature of the incident flux.

Detailed differential energy spectra were obtained with the IMP-6 for six of the eight known events occurring during the March 1971 to September 1972 lifetime of the instrument. All of these are multiple-pulse events, with several seconds separation between distinct pulses of one or two seconds duration. The pulse spectra do not obey single-

*This talk is based on an article (Cline et al., 1973) scheduled for publication in Ap. J. Letters.

index power laws in energy, but can be simply represented by exponentials in photon flux throughout the 100 to 1200 keV region. The characteristic energies at maximum intensity appear to cluster near 150 keV, with indications that departures from this value can be interpreted as circumstantial, due to attenuation when the source is at great angles from the detector axis. These burst pulses appear to ride on a softer component that exhibits a much longer decay time constant, and has a characteristic exponent near 75 keV. There is no evidence for monoenergetic line structure in the several hundred keV region, or for marked changes in the spectrum with time during a single pulse.

INSTRUMENTATION

The IMP-6 satellite was launched on 14 March 71 into an elliptic orbit with an initial apogee of over 200,000 km. Gamma-ray monitoring was provided on a nearly continuous basis, except for passes every 4.14 days through the magnetosphere, lasting several hours each. The detector was in operation from launch until 2 May 1971, and again for the period from 9 June 1971 to 27 September 1972. The instrument used consisted of a 2.25-inch diameter by 1.5-inch thick CsI(Tℓ) crystal, entirely surrounded by a thin plastic scintillator for particle rejection, viewed by a single PM tube (See Figure 1).

In addition to full-time monitoring of the rates of total intensity, particle intensity and gamma ray intensity, energy spectra of incident gamma rays were measured by a 14-channel differential analyzer with simultaneous storage in all channels. The spectra were accumulated for one half of the time, for each $\approx$ 6.3 second period from sun rise to sunset on the detector, determined by the optical aspect. This 50-percent

duty cycle resulted in missing several of the very brief intensity maxima, and two of the known gamma-ray bursts entirely. The spectral accumulation times were fixed at ≈ 5.1 seconds so that the ≈ 6.3-second live times were asynchronously split into 2 or 3 intervals of shorter durations, making possible more than one spectral determination during some of the bursts. The gain of the system was cycled through 4 positions with changes at ≈ one-week intervals for purposes of in-flight calibration; some of the bursts happended to be observed in the 69 to 1150-keV dynamic range position and some in the 53 to 880-keV range position. The primary purpose of this gamma-ray detector was use as a coincident annihilation spectrometer incorporated in a positron detector. The secondary objective was that of a solar flare monitor, and it was in this mode of operation that these unexpected gamma ray bursts were observed.

DATA OBSERVATION AND ANALYSIS

The times of occurrence of gamma ray bursts observed with multiple Vela satellite coincidences were used to identify coincident increases in the IMP-6 gamma-ray intensity. Six of the eight Vela events were observed well above the omnidirectional background, the others being missed because of the 50-percent detector duty cycle. It is possible that other events, of intensity too low to exceed the Vela threshold triggers, may also be observable with the IMP-6 instrument, and this is the subject of our next talk. Figure 2 shows the response of the IMP gamma-ray detector to the event of 30 June 1971. During a several second interval, the counts in the plastic scintillator (P) surrounding the gamma ray crystal increased by about 50, while the neutral counts

in the crystal ($\gamma\overline{P}$) simultaneously increased by about 18,000. Pulses satisfying the gamma-ray logic are fed to a multichannel analyzer, from which the outputs of three channels, added to provide the flux of 140 to 475 keV photons, indicate an increase during one $\approx$ 5-second interval of nearly 5000 counts from a total omnidirectional and secondary background of about 400 counts. This illustrates the remarkable intensity of the bursts, and shows that the response is entirely consistent with that of hard x-rays or gamma rays.

The times of occurrence and various properties of all Vela-IMP events observed during the IMP-6 experiment lifetime are listed in Table 1. The temporal structures of the observed bursts, known from the Vela results, were compared in order to determine over which intervals in the event structures the IMP spectra were obtained (See Figure 3). Since the IMP-6 satellite was spinning, an analysis was also made for each burst to determine in which direction the detector was facing, relative to the source, at the moment each spectrum was obtained. Each of the six events was observed by the Velas to have at least two distinct pulses of up to a few seconds duration, separated by intervals of several seconds. The time resolution of the IMP gamma-ray detector ($\approx$ 2.5 seconds) permitted obtaining individual spectra for many maximum-intensity pulses, and, for some cases, two separate spectra of a given several-second pulse. (Vela data show that a given maximum-intensity pulse can contain a variety of fast time variations(Klebesadel et al., 1973); these are necessarily averaged over in the IMP spectra.) Figure 4 shows photon number spectra, dn/dE, for several of the bursts, as sampled on a 6.3-second half-spin basis. It indicates that, in this energy region, relatively good fits to these raw

data are obtained to exponentials of the form $dn/dE = I_o \exp(-E/E_o)$ photons cm^{-2} keV^{-1} $burst^{-1}$. The I_o and E_o values are listed in the Table, along with the relative look direction accuracies. The directions of origin of the six events are known with widely varying accuracy, but in the case of the 30 June event, it is known that the first spectrum was recorded when the source was below the satellite horizon of the detector. Thus, the harder (250-keV) spectrum may be accounted for by attenuation of the lower-energy photons in the metal surface of the satellite. If that is also the case of the 28 March 72 event, then all the pulses are consistent with 150-keV spectra. Two of the six events (15 March 71 and 14 May 72) have unambiguously known source directions which are not far from the center of the field of view, and these are definitely 150-keV spectra. In addition, the 18 March 71 event and a number of decays of the other events, not listed, are consistent with softer spectra, suggesting that a slower-time constant, soft component is present in addition to the 150-keV peaks. Figure 5 shows the energy spectrum, or power spectrum averaged over the pulse burst duration, Edn/dE, of an event for which the source direction was known to be in the view direction. It is seen that the energy output is a maximum in this region. This may indicate that the photons released from the source objects are essentially gamma-ray in nature, not composing x-ray distributions with spectral tails in the gamma-ray region. If much softer x-rays are emitted in the primary burst they most likely undergo relatively greater absorption near their region of origin.

DISCUSSION

It is clear that the observed gamma ray bursts represent an entirely novel form of cosmic energy release. The durations of the individual pulses are typically 1 to a few seconds and the separation between pulses in a given burst are up to 20-odd seconds. The temporal structure might therefore be compared to that of solar flares, but with time scales of gamma-ray flare stars. On the other hand, the constancy of the 150-keV spectrum is a unique feature. The 150-keV energy spectra, including the one known case of the 14 May 72 event which has a power law from 10 to 100 keV (Wheaton et al., 1973), contain too much emission in the X-ray region to fit a single temperature, 150-keV black body spectrum, and yet too little emission in the lower energies to be compared to the typical, steep X-ray spectra, having power-law index of ≈ -3 or more, of most hard solar flares and many celestial X-ray sources. For those pulses which were observed with sufficient temporal resolution to obtain more than one spectrum per pulse, there is no evidence for changes in the characteristic energy during its extent (not illustrated). Further, there is no evidence for line structure in this energy region. It is possible, however, that great improvements in energy and time resolution might show fine-scale spectral variability with a variety of monochromatic lines, which average out over 2-second summations. Nevertheless, the observed constancy of a 150-keV exponential is an extremely interesting property of the bursts, which should, qualitatively at least, come out of any relevant model.

An integral size spectrum can be constructed, assuming a power law with index -1.5, normalized to 6 or 8 events per 1.5 years with sizes greater than 10^{-4} erg cm^{-2} for the energy region above 100 keV. Since

the 18 known events have source directions compatible with isotropy (Strong and Klebesadel, 1973), this size spectrum can be arbitrarily normalized in order to obtain upper limits of the frequencies of occurrence of smaller events. In the case of extragalactic sources, a summation of all emission up to cosmological distances produces a total isotropic background intensity upper limit which is below the presently observed diffuse cosmic background in this 100 to 1200 keV energy interval. Thus an extragalactic origin cannot be ruled out. Further, if all sources have spectra with $\simeq$ constant 150-keV exponentials, then the total cosmic spectrum will not extend into the several MeV region with sufficient intensity to explain the bump in the diffuse cosmic background observed (Trombka et al., 1973) at those energies.

References

Cline, T. L., Desai, U. D., Klebesadel, R. W., and Strong, I. B., 1973, Ap. J. Letters, October 1 issue.

Klebesadel, R. W., Strong, I. B., and Olson, R. A., 1973, Ap. J. Letters 182, L85.

Strong, I. B., and Klebesadel, R. W., 1973 (in preparation).

Trombka, J. I., Metzger, A. E., Arnold, J. R., Matteson, J. L., Reedy, R. C., and Peterson, L. E., 1973, Ap. J. 181, 737.

Wheaton, W. A., Ulmer, M. P., Baity, W. A., Datlowe, D. W., Elcan, M. E., Peterson, L. E., Klebesadel, R. W., Strong, I. B., Cline, T. L., and Desai, U. D., 1973 (submitted for publication).

EVENT	BURST	I_o	E_o	
15 Mar 71	Second Max	1.9	156	Includes Source ($\alpha \approx 50°$, $\delta = -30 \pm 10°$)
18 Mar 71	Decay of 1st	1.8	74	Spins through Source
30 Jun 71	First Max	0.7	276	Source below satellite horizon
30 Jun 71	Second Max	5.5	142	Spins through Source
30 Jun 71	Decay of 2nd	0.7	110	Spins through Source
17 Jan 72	Decay of 1st	0.10	138	Source position undetermined
17 Jan 72	Second Max	0.35	184	Source position undetermined
17 Jan 72	Decay	0.11	170	Source position undetermined
28 Mar 72	First Max	0.50	238	Source near or below horizon
28 Mar 72	Second Max	0.55	176	Source position undetermined
14 May 72	First Max	0.8	166	Includes Source ($\alpha \approx 175°$, $\delta \approx +77°$)
14 May 72	Second Max	0.8	152	Includes Source

Table 1. Characteristics of gamma-ray burst spectra.

Exponential fits in dn/dE provide I_o in units of photons cm^{-2} keV^{-1}, and E_o in units of keV, both of which have systematic uncertainties depending on relative look angle.

Figure Captions

Figure 1. The gamma ray detector is the central system in this array of three scintillator-photomultiplier combinations used on IMP-6 for electron-positron studies.

Figure 2. The response of the detector to a gamma ray burst, as indicated by the plastic anticoincidence (P), the CsI gamma ray detector ($\gamma\overline{P}$) and several channels added to give the 140 to 475 keV photon rate, where the gamma-ray energy response is maximized. Each point samples two differential energy spectra.

Figure 3. Time histories of the observed bursts, plotting the response of only one differential energy channel. The detector is turned on for one-half the time. Comparison with Vela data made possible the identification of when the burst intensity maxima occurred.

Figure 4. Number spectra, dn/dE, of several bursts, selected for a variety of responses. The two 250-keV spectra are interpreted as due to attenuation by the satellite material in cases where the source was below the detector horizon; the 70-keV spectrum is from the decay phase of an event. The $\approx$ 150-keV sample spectra are from intensity maxima observed directly.

Figure 5. The energy spectrum, E dn/dE, of a directly observed event.

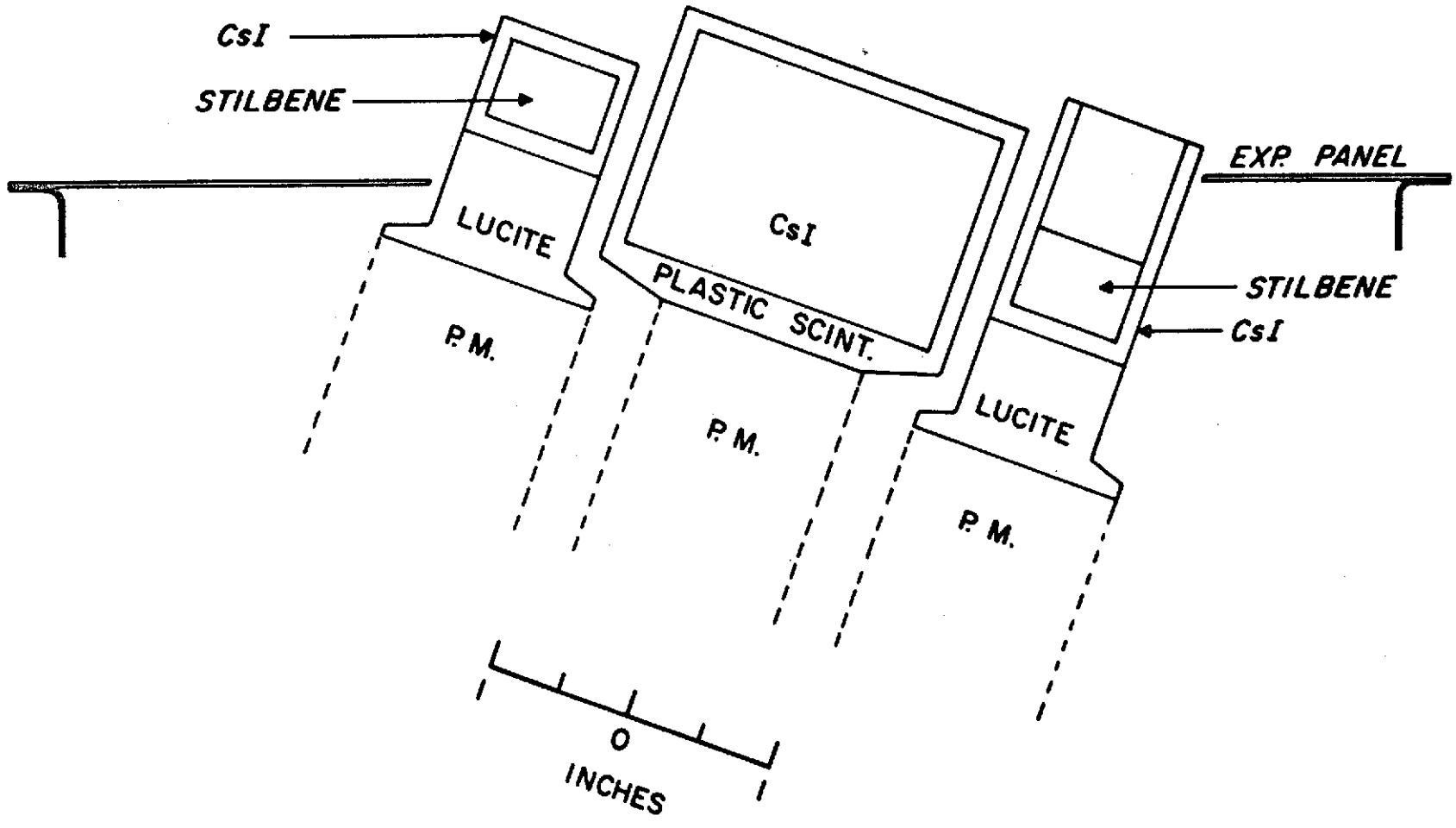
CsI
STILBENE
LUCITE
P.M.
CsI
PLASTIC SCINT.
P.M.
EXP. PANEL
STILBENE
CsI
LUCITE
P.M.
0
INCHES

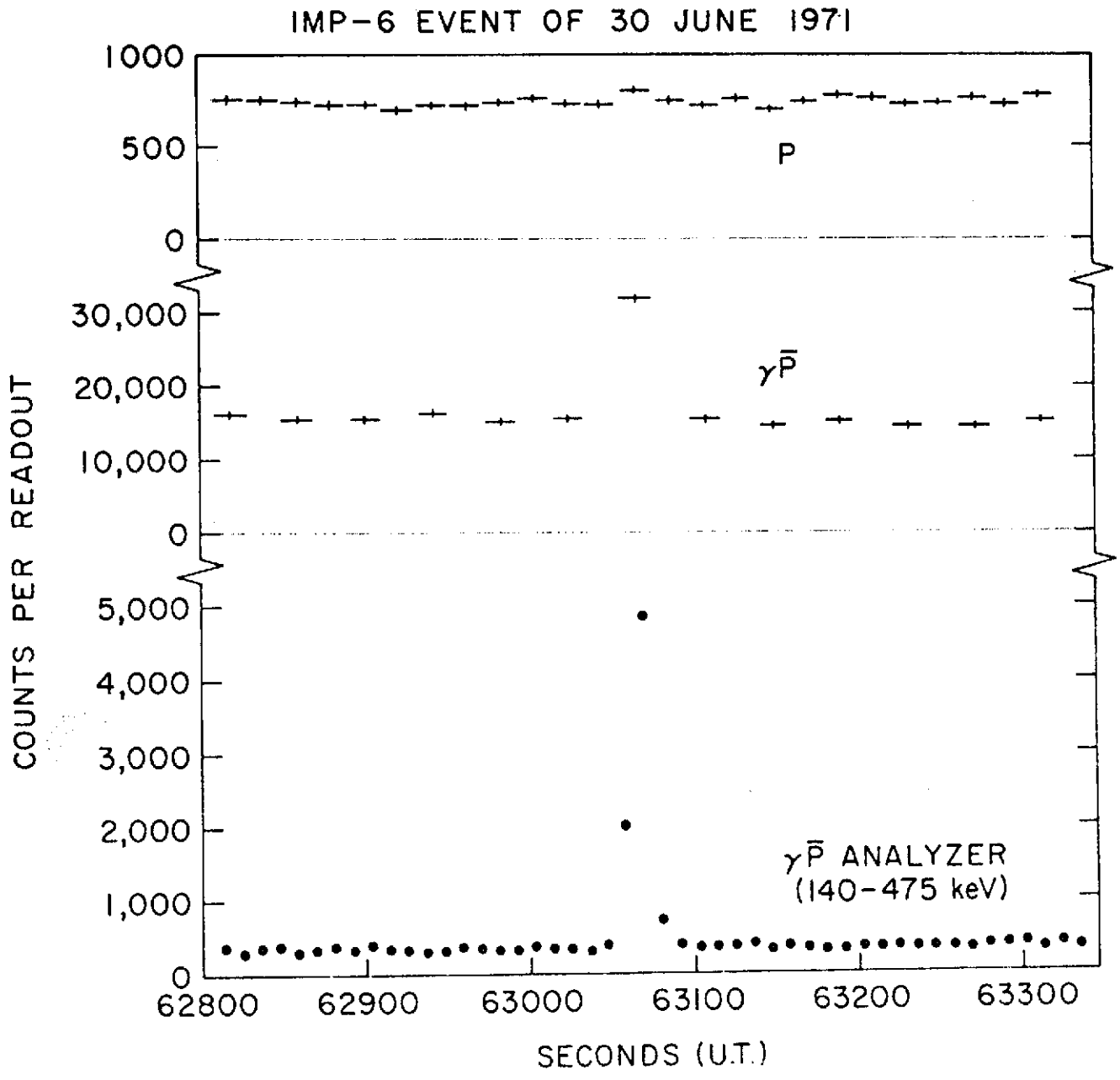
IMP-6 EVENT OF 30 JUNE 1971
1000
500
0
P
30,000
20,000
10,000
0
$\gamma\bar{P}$
5,000
4,000
3,000
2,000
1,000
0
$\gamma\bar{P}$ ANALYZER
(140-475 keV)
COUNTS PER READOUT
62800
62900
63000
63100
63200
63300
SECONDS (U.T.)

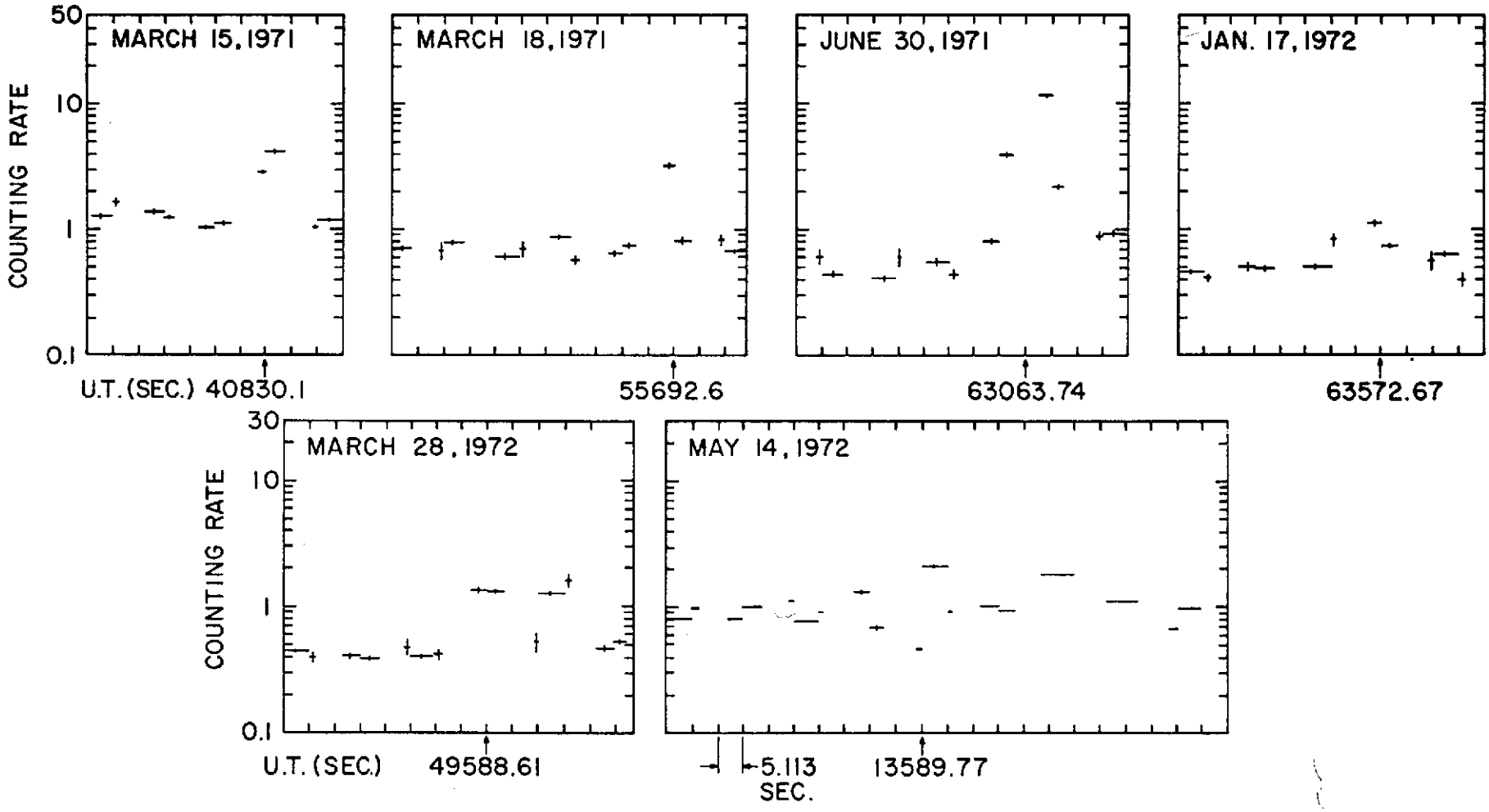
50
10
1
0.1
COUNTING RATE
MARCH 15, 1971
MARCH 18, 1971
JUNE 30, 1971
JAN. 17, 1972
U.T. (SEC.) 40830.1
55692.6
63063.74
63572.67
30
10
1
0.1
COUNTING RATE
MARCH 28, 1972
MAY 14, 1972
U.T. (SEC.)
49588.61
5.113
SEC.
13589.77

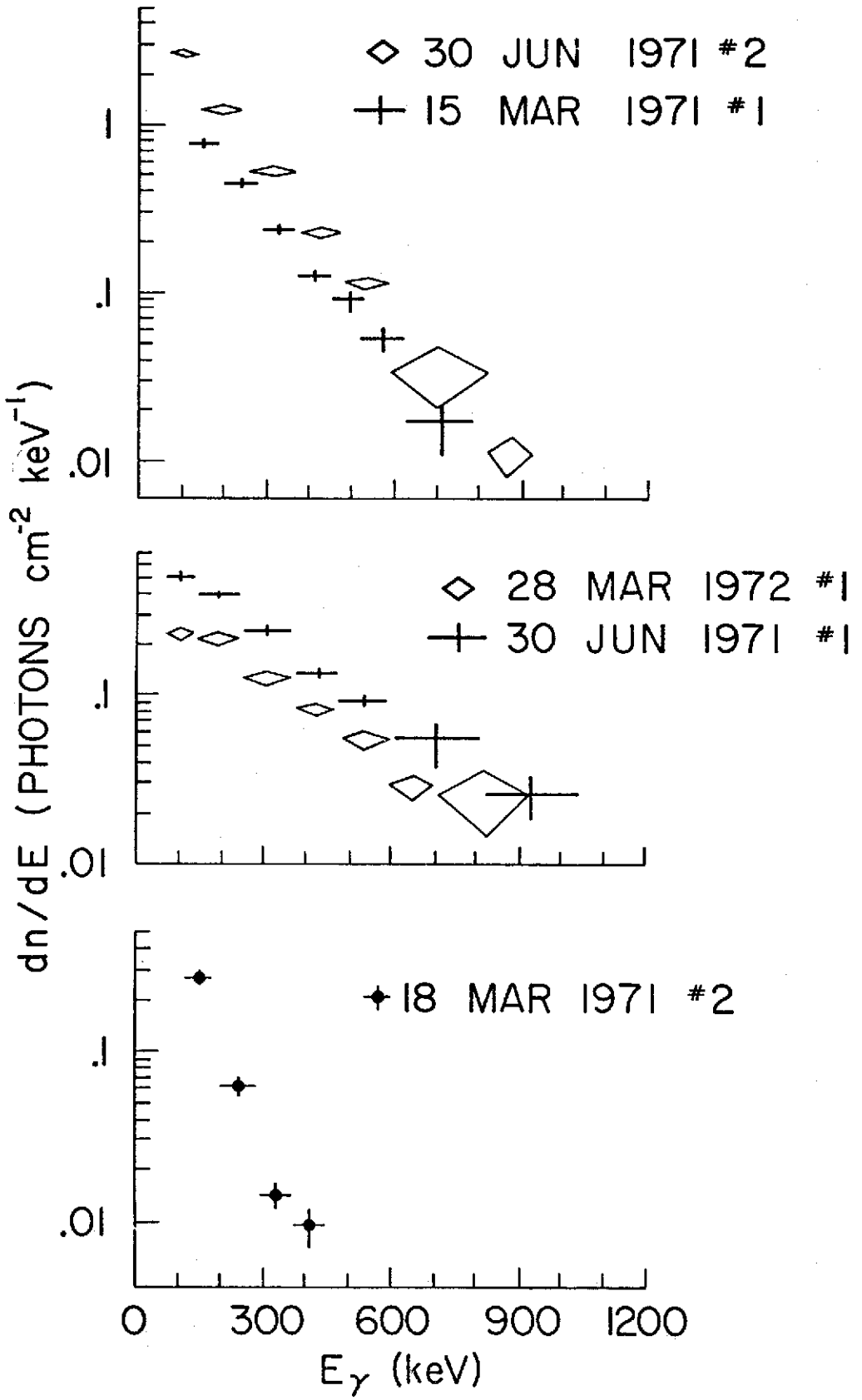
30 JUN 1971 #2
15 MAR 1971 #1
28 MAR 1972 #1
30 JUN 1971 #1
18 MAR 1971 #2
dn/dE (PHOTONS cm⁻² keV⁻¹)
1
.1
.01
0
300
600
900
1200
Eγ (keV)

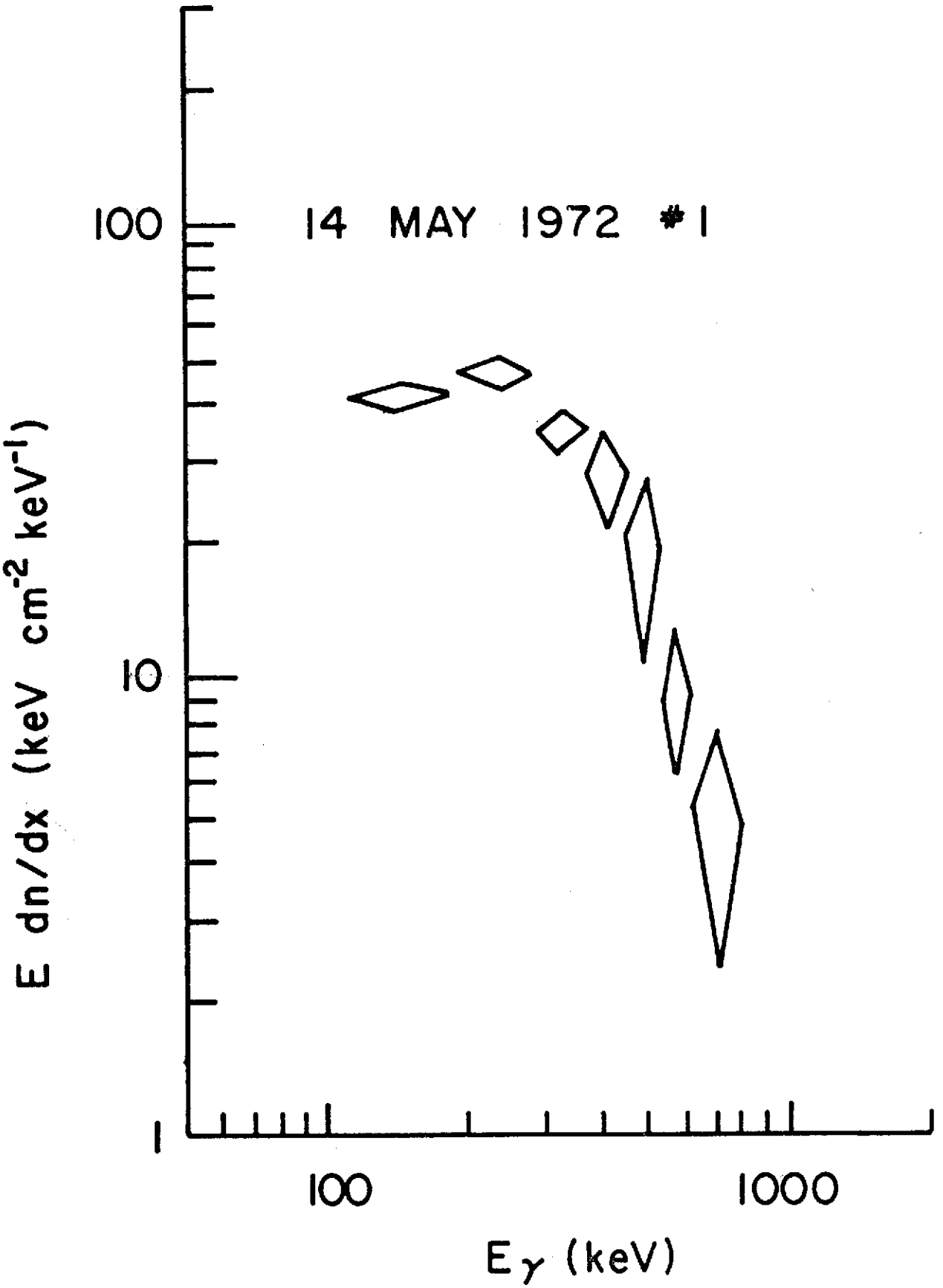
14 MAY 1972 #1
100
10
1
E dn/dx (keV cm^{-2} keV^{-1})
100
1000
E_γ (keV)

N74-11611

IMP-6 OBSERVATIONS OF SMALL-SIZED CANDIDATE COSMIC GAMMA-RAY BURSTS

T. L. Cline and U. D. Desai
NASA/Goddard Space Flight Center
Greenbelt, Maryland 20771

A talk presented at the Los Alamos Conference on Transient Cosmic Gamma- and X-Ray Sources, September 20, 1973, delivered by T. L. Cline.

The purpose of this short contribution is to point out that observations from IMP-6 may make possible the detection of a number of cosmic gamma-ray bursts in addition to those previously cataloged by the Los Alamos observers. At the present time, it is still the case that no cosmic gamma-ray bursts, detected by two or more satellites, have not been observed by the Velas. The IMP-6 detector is, however, sensitive to events considerably smaller than those which exceed the Vela thresholds, as evidenced by the fact that those six events we have observed are more than an order of magnitude, and up to several hundred standard deviations, above background. If the size spectrum goes as $S^{-1.5}$, as it would for an extended source region with no immediate cutoff, then we might have detected as many as $(10^{1.5}) \times 4 \times 1.5 \times 0.75 = 140$ in the one and a half years of IMP-6 observation, assuming a 75 per cent effective duty cycle, given a rate of 4 large events per year. Even if this is based on an optimistic evaluation of our signal to noise separation, the number of expected events is certainly very large compared with 6.

In the present state of the art, one cannot claim to be detecting gamma-ray bursts without having a coincidence between separate satellites, but there is some merit to compiling a list of single-satellite candidate events. First, other satellites (such as OGO-5, OSO-7, TD-1, etc.) may provide coincident observations during times of overlap, in order to unambiguously identify events. Second, even without coincident detection, a size spectrum of candidate events will be useful if it turns out to be below, rather than above, the expected size spectrum extrapolated from existing data. Clearly, in the limiting case, if IMP-6 should be sensitive to about a hundred events per year, and yet produces a much smaller number of candidates, then the size spectrum of real events must contain a cutoff. Third, the azimuthal distribution of these IMP-6 candidate events can be determined to search for an anisotropy. If not too many erroneous events are included (such as solar flares, noise bursts, etc), then a visible anisotropy would be informative.

At present we are completing a computer program to search for and identify these candidate events. Selection criteria are based only on consistent time scale and observable intensity. Rise time considerations are not included, of course, since our temporal resolution is several seconds; thus any comparably sized events that are missed by the Velas on this basis will be detectable. In addition, the use of the differential energy analyzer with simultaneous storage makes possible a search for intensity increases simultaneously in several channels. The apparent energy spectrum of each candidate burst can be examined in order to compare

against the known spectra of multiply detected events.

So far, only 25 percent of the raw data have been exhaustively scanned, using a preliminary version of this program. A number of candidate events have been seen which possess the appropriate time scales and energy spectra. Three candidate events which occurred during the unusually short time span of several days are shown plotted in Figure 1. The average rate of occurrence during the first several months seems to be lower than expected, but detailed calculations will be required to quantitatively determine whether such is the case. The azimuthal sensitivity of the IMP-6 detector must be taken into account, as well as the dead time. These effects will alter the absolute intensity of the resulting size spectrum, without changing its spectral shape. All the available data collected over one and a half years will be used before any analysis is presented, to avoid unnecessarily poor statistical results. The optimistic note is that the apparent rate of occurrence of candidate burst is not greater than it should be, based on the $S^{-1.5}$ model. This indicates that, at most, few spurious events are included, and implies that the ultimate result of this search may be quantitatively useful.

Figure Captions

Figure 1. The energy spectra of three of the largest candidate bursts. These three were detected in an unusually short period of time compared with the average rate of occurrence of candidate events of this size.

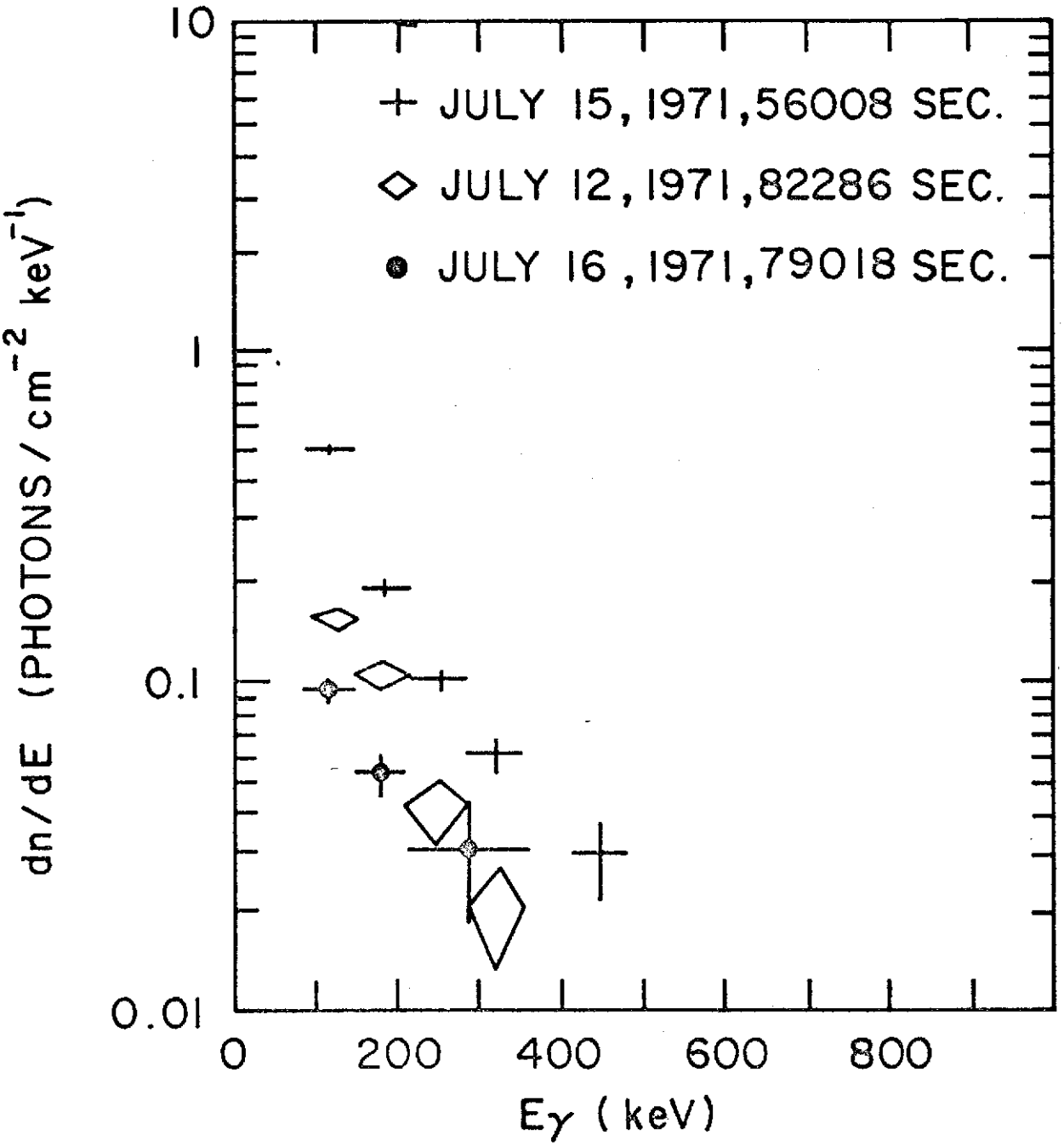
10
1
0.1
0.01
+ JULY 15, 1971, 56008 SEC.
◇ JULY 12, 1971, 82286 SEC.
● JULY 16, 1971, 79018 SEC.
dn/dE (PHOTONS / cm⁻² keV⁻¹)
0
200
400
600
800
Eγ (keV)

A DIRECTIONAL LOW ENERGY GAMMA-RAY DETECTOR

G. Morfill and G. F. Pieper*

Max Planck Institüt für Extraterrestrische Physik
8046 Garching bei München, W. Germany

*Permanent address: Goddard Space Flight Center
Greenbelt, Maryland U.S.A. 20771

N74-11612

Abstract

The sensitivity of a directional gamma-ray detector, which relies on blocking a source to determine its direction and energy spectrum, is calculated and compared to the more conventional well-shaped shielded detectors. It is shown that such an 'anticollimator' detection system provides a basis for measuring the celestial diffuse gamma-ray background, gamma-ray sources and bursts with good energy, angular, and time resolution, and that additionally the system is 20 to 50 times as sensitive as conventional detectors when compared on a per unit mass basis.

Introduction

Important outstanding problems in gamma-ray astronomy today are the accurate determination of the diffuse gamma-ray background and its degree of isotropy[1], the location and energy spectra of possible gamma-ray sources[1], and measurement of the energy spectra of bursts[2] which are possibly due to emissions from flare stars[3].

The experimental requirements for the three areas of research mentioned above are different; the background measurement requires a good knowledge of the detector efficiency and spacecraft absorption and background, as well as the long-time accumulation of data, the anisotropy and source measurements require the detector to have good directionality which is then employed in an all-sky survey, and the measurements of bursts require in addition to directionality good temporal resolution.

It can be shown that a single experimental setup, which relies on an anticollimation technique, provides optimum or near optimum possibilities for new measurements in the above problem areas.

Description of the Detector Concept

This paper describes a directional low energy gamma-ray detector (> 200 keV to < 30 MeV) of high sensitivity. Gamma rays in the energy range discussed have very small absorption coefficients, even in detectors of high atomic mass (e.g. CsI or NaI), so that large amounts of scintillator are needed to absorb them.

The merits of the detector outlined below are summarized as follows:

1) The detector is highly directional ($\sim 6^{o}$) and can resolve closely-spaced sources.
2) The detector is able to measure the diffuse omnidirectional background since it does not have a collimator and, therefore, a complicated transmission function. Thus it is possible to measure sources and background both efficiently with the same instrument.
3) Compared to conventional detectors (active collimator systems) an increase in sensitivity of a factor 20 - 50 is achieved for the same detector mass in the important energy range 1 MeV - 15 MeV.
4) The detector consists of six independent units, and has, therefore, a large degree of redundancy without affecting detector performance significantly (15% reduction in sensitivity if one unit fails).

5) Modulation of the source is achieved five times for each unit during a satellite spin period, so that time variation (due to e.g. solar X-ray events) in the background flux can be eliminated.

6) Fast time resolution is required for scanning directionality, with data accumulated in various spin sectors (e.g. 120 sectors 3^{o} wide). It is easy to compare the total measured counting rate during such a spin sector with a (variable) threshold level, for separate storage in the case of an anomalous increase in intensity.

The detector suffers from induced radioactivity background[4] just like any other alkali halide detector system which does not rely on coincidence measurement. In order to obtain maximum sensitivity and minimum background due to this source, an orbit similar to that of ERS 18 (perigee 3 R_E, apogee 18 R_E) is required, or alternatively an equatorial low altitude (< 450 km) orbit, which always remains below the radiation belt may be used. Atmospheric gamma rays might be a further source of background in the low altitude orbit, and would make measurement of the diffuse flux more difficult.

Measurements of radiations from distant astronomical sources usually involve orienting a detection device to intercept a parallel beam of the radiation. Frequently the detection device is sensitive to background radiations from other than the desired direction, necessitating that a shielding material be placed around the detector to absorb radiations from all directions except the desired one. In the case of visible

light or other easily absorbed radiations, a passive shield can be used with little weight penalty. For X- and gamma-rays of a penetrating nature, an active shield must be used in anticoincidence with the detector to eliminate radiations partially absorbed in the shield (e.g. Compton scattered) or secondary effects (e.g. K-X-rays). Such a shield can impose a severe weight penalty on the detector system and can still serve as a source of additional background from the decays of radioactivities created in the shield.

An alternate system, which may be called an "active anticollimator" has been suggested[5,6]. Its properties turn out to be considerably more satisfactory for low energy gamma rays (0.1 ~ 10 MeV) than those of an active collimator. The active anticollimator (AAC) consists of an array of n identical alkali halide detectors arranged in a regular manner evenly spaced along the circumference of a circle. (See Fig. 1.) Each detector crystal is a cylinder R cm in radius and 2R high. The axes of the cylinders are all parallel to each other, perpendicular to the plane of the circle. The whole system rotates about an axis through the center of the circle, also perpendicular to the plane of the circle. Imagine the spin axis of the system oriented so that radiation from the source being investigated enters in the plane of the circle.

Then each detector will be blocked successively by the other detector crystals and a modulation of its counting rate will occur. We wish to determine the amplitude of this modulation and to compare the AAC system to the AC system on a per unit mass of detector basis.

1) AAC System

We consider first, for simplicity, a two-detector system, consisting of two spherical detectors of radius R separated by a distance M. For additional simplicity in presentation, we assume here that all radiations pass through the center of each spherical crystal. (The situation is changed quantitatively (~ 30%), but not qualitatively when off-center radiations are included.) We shall measure the number of counts, N_S, from a distant source of energy spectrum $F_S(E)$ $\frac{\text{photons}}{\text{cm}^2 \text{ sec MeV}}$ in a time Δt when the source can be seen clearly by one detector and the number of counts, N_S', in an equal interval Δt when the source is occulted by ther other detector. In both cases, an isotropic background of spectrum $F_B(E)$ $\frac{\text{photons}}{\text{cm}^2 \text{ sec ster MeV}}$ will produce N_B counts in Δt. For the modulation to be significant to 3 standard deviations, the difference between the occulted and non-occulted numbers of counts must satisfy the ratio

$$R_a = \frac{N_S + N_B - N_S' - N_B}{[N_S + N_B + N_S' + N_B]^{1/2}} \geq 3 \qquad (1)$$

In the energy interval ΔE, we have

$$N_S(E)\ \Delta E = F_S(E)\ \pi R^2\ \Delta t\ (1 - e^{-2\mu(E)R})\ \Delta E \qquad (2)$$

$$N_S'(E)\ \Delta E = F_S(E)\ \pi R^2\ \Delta t\ (1 - e^{-2\mu(E)R})e^{-2\mu(E)R}\ \Delta E \qquad (3)$$

and

$$N_B(E)\ \Delta E = F_B(E)\ \pi R^2\ \Delta t\ (4\pi - d\Omega + d\Omega^{-2\mu(E)R})\ (1 - e^{-2\mu(E)R})\ \Delta E \qquad (4)$$

where $\mu(E)$ is the linear absorption coefficient for gamma radiation in the detector and $d\Omega = \pi R^2/h^2$ is the solid angle subtended by one detector at the other. It is a good assumption in all cases that $d\Omega << 4\pi$. We also assume N_S and N_S' are $<< N_B$ (or $4\pi F_B >> F_S$). With these assumptions, the ratio becomes

$$R_a = \frac{F_S\sqrt{\Delta t}}{2\sqrt{2F_B}}\ R\ (1 - e^{-2\mu R})^{3/2} \qquad (5)$$

It is easy to extend this calculation to the case of n detectors in a regular array, as in Fig. 1. Since the source can either be seen by a given detector or be occulted by only one other detector at one time, neither N_S nor N_S' is changed. The background count N_B is changed by replacing $d\Omega$ by $n \cdot \overline{d\Omega}$, but the final result for R_a remains unchanged if $n \cdot \overline{d\Omega} << 4\pi$ remains a valid assumption.

The effect of additional detectors is felt in the time. Out of a total viewing time T (= many system spin periods), source occultations with n detectors occur for a time $\Delta t = \frac{\bar{\alpha}}{360} \cdot T \cdot n \cdot (n-1)$, where $\bar{\alpha}$ is the mean full width at half maximum angle subtended by one detector at another. We may now write for R_a

$$R_a = \frac{F_S \sqrt{\frac{\bar{\alpha}}{360} T}}{2\sqrt{2 F_B}} \sqrt{n(n-1)} \; R \left(1 - e^{-2\mu R}\right)^{3/2} \qquad (6)$$

from this we define G, the geometric factor for an array of n detectors of radius R

$$G = \sqrt{n(n-1)} \; R \left(1 - e^{-2\mu R}\right)^{3/2} \qquad (7)$$

Figures 2 and 3 show the properties of this factor as a function of μ, R, and n. In all cases, the variable n or R is suppressed in favor of the total volume of the detector system in order to facilitate later comparison with the AC system. Fig. 2 shows the effect of increasing the number of detector spheres at an intermediate value of μ, and Fig. 3 shows the dependence of G on volume for a system of 6 spheres at various values of μ. The effect of the nearly total absorption of incoming radiation at large radius and high μ is clear. It turns out that a system of 6 detectors appears most reasonable if detectors identical to the Apollo 15 and 16 detectors are used ($R \cong 4.5$ cm) and the enveloped arrangement is confined to a Scout shroud size.

2. AC System

The active collimator (AC) system is shown in Fig. 4. The analysis is similar to that for the AAC. When the source is visible in the detector opening,

$$N_S(E)\ \Delta E = F_S\ (E)\ \pi\ (R-x)^2\ \Delta t\ (1-e^{-2\mu(R-x)})\ \Delta E \qquad (8)$$

when the source is invisible,

$$N_S'(E)\ \Delta E = N_S(E)\ e^{-\mu x}\ \Delta E \qquad (9)$$

In both cases, the background counts will be

$$N_B(E)\ \Delta E = F_B(E)\ \pi\ (R-x)^2\ \Delta t\ (1-e^{-2\mu(R-x)})$$

$$(dr + (4\pi - d\Omega)\ e^{-\mu x})\ \Delta E \qquad (10)$$

Here again $\mu = \mu(E)$, and $d\Omega = \pi\ (R - x)^2/l^2$ is the solid angle of opening of the AC. Using the same assumptions as previously, $d\Omega << 4\pi$ and $4\pi\ F_B >> F_s$,

$$R_a = \frac{F_s\sqrt{\Delta t}}{2\sqrt{2\ F_B}}\ (R-x)\ (1-e^{-2\mu(R-x)})^{1/2}\ (1-e^{-\mu x})\ e^{\mu x/2} \qquad (11)$$

The geometric factor for this system is then

$$G = (R-x)\ (1 - e^{-2\mu(R-x)})^{1/2}\ (1 - e^{-\mu x})\ e^{\mu x/2} \qquad (12)$$

It is necessary first to optimize the value of x. Fig. 5 shows this optimization, plotting G vs. x for constant μ. When μ is small, the maximum in G is very flat, so it would be quite acceptable in practice to choose a constant value of x for all μ appropriate to a higher value of μ. In the calculations actually done, the optimum value of x was used for each value

of μ. The properties of the AC system as a function of detector volume for various values of μ are shown in Fig. 6. This figure shows that the AC system has large values of G only for large μ and large volumes.

Comparison of AC and AAC Systems

1. Sensitivity

The AC and AAC systems are compared in Fig. 7, for an AAC system of 6 spheres of radii 3, 4, or 5 cm, each with an AC system of approximately equal volume, i.e., the AAC system of 6 spheres of R = 4 cm has a volume of 1608 cm^3 and should therefore be compared with the AC system of R = 5 cm, whose volume is 1586 cm^3, etc. In each case, the clear superiority of the AAC system at lower values of μ is evident. It is also clear that at higher values of μ than shown in Fig. 7, the AC system will have the advantage, e.g. at ~ 40 kev the AC system will be superior, corresponding to the active shield's being a real total absorber and removing the background. Thus the AC and AAC systems are complementary, with the cross over point between them being approximately 200 kev, where the photoelectric absorption becomes small.

We wish now to compare the AC and AAC systems against the radiation from a known source, the Crab Nebula, whose energy spectrum is given quite accurately by

$F_s(E) = 0.9 \times 10^{-2} E^{-2} \frac{\text{photons}}{\text{cm}^2 \text{ sec MeV}}$. For a 3 standard deviation observation, we have

$$F_s^* = \frac{6\sqrt{2 F_B}}{G\sqrt{\frac{\bar{\alpha}}{360}\,T}} \tag{13}$$

where F_s^* is the minimum resolvable photon flux from a source. We take[1] $F_B = 0.026 E^{-2}$ photons/cm^2 sec ster MeV, thus

$$F_s^* = \frac{26}{G \cdot E\sqrt{\bar{\alpha}T}} \tag{14}$$

with $\bar{\alpha}$ in degrees, T in seconds, E in MeV and G in cm. Choosing $\bar{\alpha} = 7^o$ and T = 1 day = 8.64×10^4 sec, we have

$$F_s^* = \frac{3.34 \cdot 10^{-2}}{E \cdot G(E)} \tag{15}$$

The results for an AAC system of R = 4 cm, n = 6 spheres, ($\therefore$ volume = 1608 cm^3) for both NaI and CsI are shown in Fig. 8 along with the result for an AC system of comparable volume ($\approx$ 1586 cm^3). The results show that the Crab should

be observable to about 3.7 MeV (a flux of $\sim 7 \times 10^{-4}$ photons/cm^2 sec MeV) using an AAC system of R = 4 cm, n = 6, and thus volume 1608 cm^3, a mass therefore of 7.25 kg CsI. The AC system can see the Crab above background only to 600 kev (a flux of $\sim 2.5 \times 10^{-2}$ photons/cm^2 sec MeV) with an approximately equal volume, 1586 cm^3, and a mass of 7.15 kg CsI.

@. Angular and Energy Resolution

The spacing of some of the strongest X-ray sources near the galactic center is close enough to require an angular resolution of $\sim 5^o$ to 7^o at full width half maximum, in order to resolve them. Both detector systems (AC and AAC) were therefore chosen to have angular resolutions of 7^o FWHM. (Counts in the AAC detector should be accumulated in spin sectors of angular width $\leq$ 1/2 times the detector angular resolution, i.e. in this case $\sim 3^o$. This is necessary in order not to smear out the modulation in detector counting rates introduced by source occultation. If the satellite spin rate is w revolutions/minute, the time spent in accumulating data in the same spin sector of 3^o width is $\frac{1}{2w}$ seconds during one satellite revolution.)

Modulations in count rate due to an uneven mass distribution in the spacecraft can be detected in the AAC system (a single detector system would not be able to do this) and can be removed, as they would not, in general, have the same characteristics as a source modulation.

Energy resolution depends on the crystal size; a large crystal will minimize electron escape and lead to a larger photopeak, especially for incident gamma rays of high energy. The AAC system employs larger detecting crystals than the optimum design AC system of the same mass. Thus the energy resolution of the AAC system should be better at large energies than that of the AC system, although the active shield will reduce the size of the Compton plateau in the latter system and thus emphasize the importance of the photopeak again. At ~ 10 MeV energies, the AC system will become very inefficient due to high energy electron escape.

3. Burst Detection

The observed gamma-ray bursts[2] last for times up to ~ 30 seconds during which the X-ray counting rates have exceeded the background rates by factors of 10 or more. Clearly it is important to measure accurately the direction of arrival of these photons as well as their energy spectra in order to learn something about their origin. This requires a fast reaction time to measure a statistically significant increase in the counting rate. The fastest time division required for angular resolution is the accumulation time during one spin sector, i.e. $\frac{1}{2w}$. This interval may be subdivided further for the purposes of fast burst detection. Comparison of the total integrated count rates of all crystals in the AAC with a programmable reference rate should ensure that bursts can be

detected within a small fraction of a second and that the period of enhanced counting rate during the burst is stored separately for energy spectral analysis. If the 'burst' radiation lies in AAC system plane, its direction can be determined to an accuracy of a few degrees, if the burst lasts longer than $\frac{1}{w}$ seconds, where w is the spacecraft spin rate in revolutions/sec. If the sources of these bursts are randomly spaced, the probability of one of them being observed while it is coplanar with the AAC system (within the detector resolution) is given by

$$P = \frac{\bar{\alpha} \cdot 2\pi}{4\pi} = \frac{\bar{\alpha}}{2} \qquad (16)$$

For $\bar{\alpha} = 7^{o}$, $P \approx 3\%$. It is likely that many of these gamma ray burst sources lie in the galactic plane, thus P should be substantially greater than 3% during a galactic plane scan, which would initially fix such source locations to within a few degrees with a single AAC detection system. Greater angular resolution can be obtained by triangulation of path lengths using several well separated spacecraft.

Conclusions

We have shown that a gamma-ray detector system can be constructed, which works on an anticollimation principle (AAC) and which has good properties for the measurement of the diffuse celestial background gamma-ray energy spectrum, the measurement of the energy spectra of discrete sources including the recently observed gamma-ray bursts. The system has good sensitivity, angular, energy and time resolution.

References

(1) Proceedings of the International Symposium and Workshop on Gamma-Ray Astrophysics, Goddard Space Flight Center, preprint X-641-73-180, June 1973.

(2) Klebesadel, R. W., I. B. Strong and R. A. Olsen, Astrophys. J. Lett. 182, L85, 1973.

(3) Stecker, F. and K. Frost, Nature, to be published, 1973.

(4) Dyer, C. S. and G. E. Morfill, Astrophysics and Space Science 14, 243, 1971.

(5) Morfill, G. E., Ph.D. Thesis, Imperial College of Science and Technology, London, 1971.

(6) Morfill, G. E. and G. F. Pieper, Jahresbericht 1972, Max-Planck Institut fur Extraterrestrische Physik, Garching b. Munchen, W. Germany.

Figure Captions

Figure 1 Schematic diagram of the active anti-collimator detector assembly, viewed from an angle above the rotation plane. A is the absorber and D the detector crystal for the source position shown.

Figure 2 Active anti-collimator 'geometric factor' G (see text), which is a measure of detector sensitivity, as a function of total detector volume (proportional to detector mass). 'n' is the number of crystals used, and μ (cm^{-1}) is the absorption coefficient. This figure shows that asymptotically, G increases linearly with detector volume, independent of n, the number of detectors. It is then more efficient to increase n rather than the size of the individual crystals.

Figure 3 'Geometric factor' G (see text) for the active anti-collimator case of six crystals, discussed in the text, as a function of total detector volume and absorption coefficient μ (cm^{-1}).

Figure 4 Diagram of the active collimator (AC) assembly chosen for comparison with the active anticollimator (ACC) system. l is the length of the collimator, h_{pm} the height of the inside photomultiplier (taken to be 5 cm).

Figure 5 'Geometric factor' G (see text) for the active collimator at various absorption coefficients μ. This figure shows that, at given μ, an optimum collimator thickness can be calculated which yields the greatest sensitivity (largest G). The total detector mass has been held constant (R = 5 cm).

Figure 6 'Geometric factor' G (see text) for the optimum design (see Figure 5) active collimator (AC) system as a function of total detector volume. G is plotted for various absorption coefficients u (cm^{-1}) as in Figure 3 for the case of the active anticollimator. Note the very slow increase in sensitivity for low u values even for volumes corresponding to very large detector masses.

Figure 7 Comparison of active collimator (AC) and active anticollimator (AAC) sensitivities as a function of absorption coefficient μ. This figure shows that the AAC system increases in sensitivity more rapidly at low μ (< 0.4 cm^{-1}) than the AC system, whereas at larger μ (> 0.5 cm^{-1}) this situation is reversed. Thus the AAC system is more sensitive in the gamma ray region.

Figure 8 Comparison of the sensitivities of an optimum design active collimator (AC) with an active anticollimator system (AAC) consisting of 6 right circular cylinders of length and diameter 8 cm. The minimum detectable source strength to 3 standard deviations is shown, as well as the extrapolated Crab X-ray spectrum for comparison.

Active Anticollimator

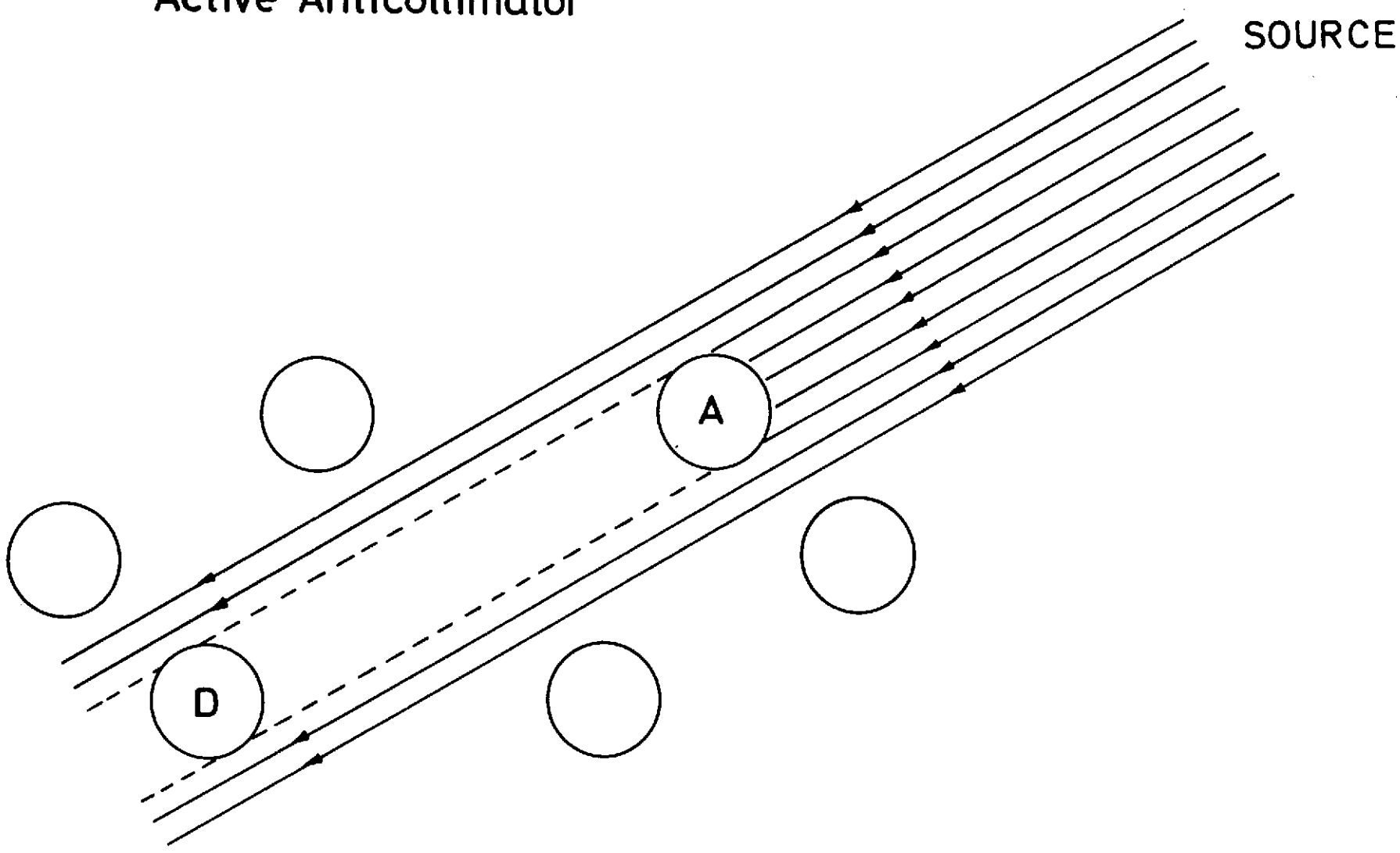

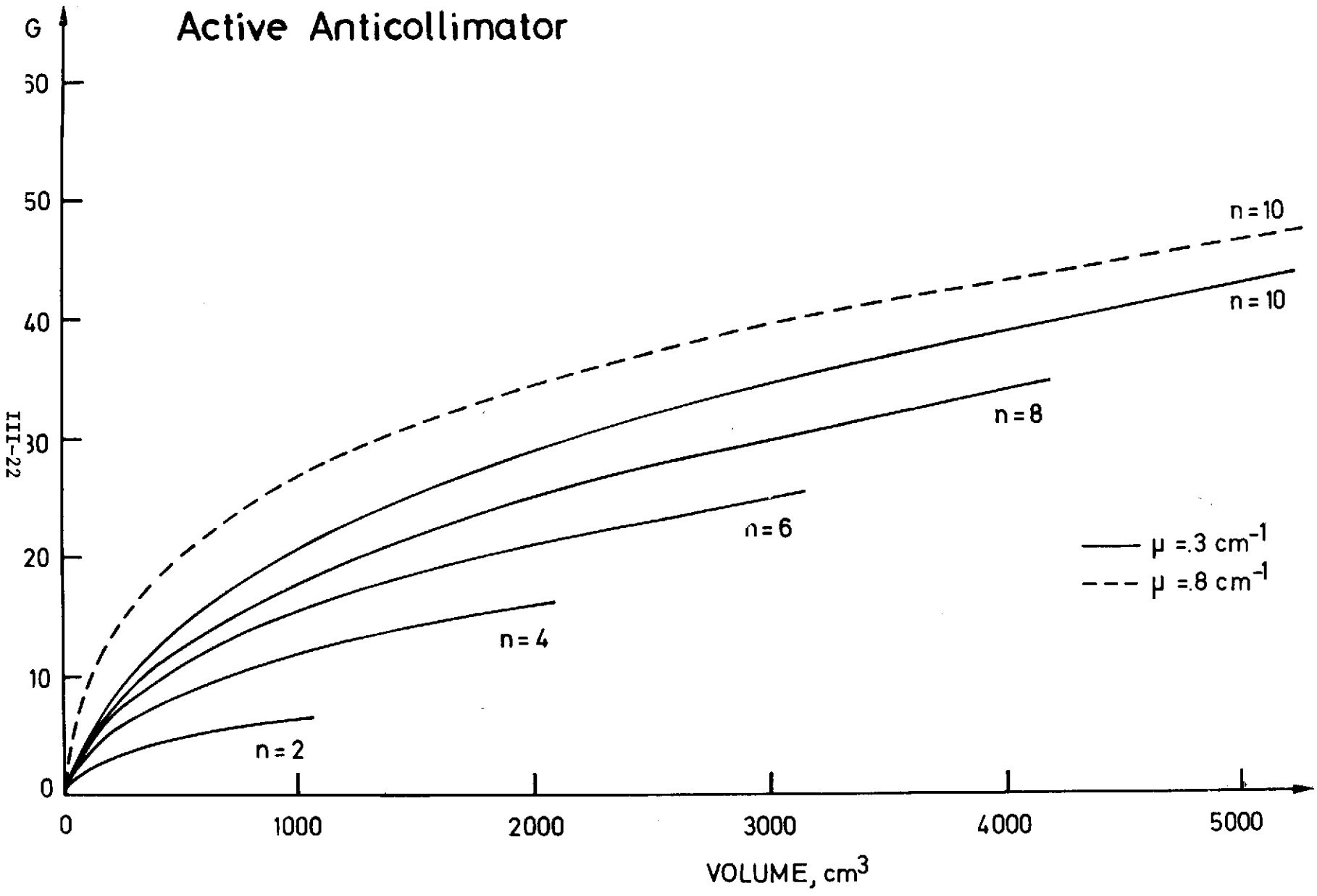
Active Anticollimator
G
50
40
30
20
10
0
n = 10
n = 10
n = 8
n = 6
n = 4
n = 2
μ = .3 cm⁻¹
μ = .8 cm⁻¹
0
1000
2000
3000
4000
5000
VOLUME, cm³

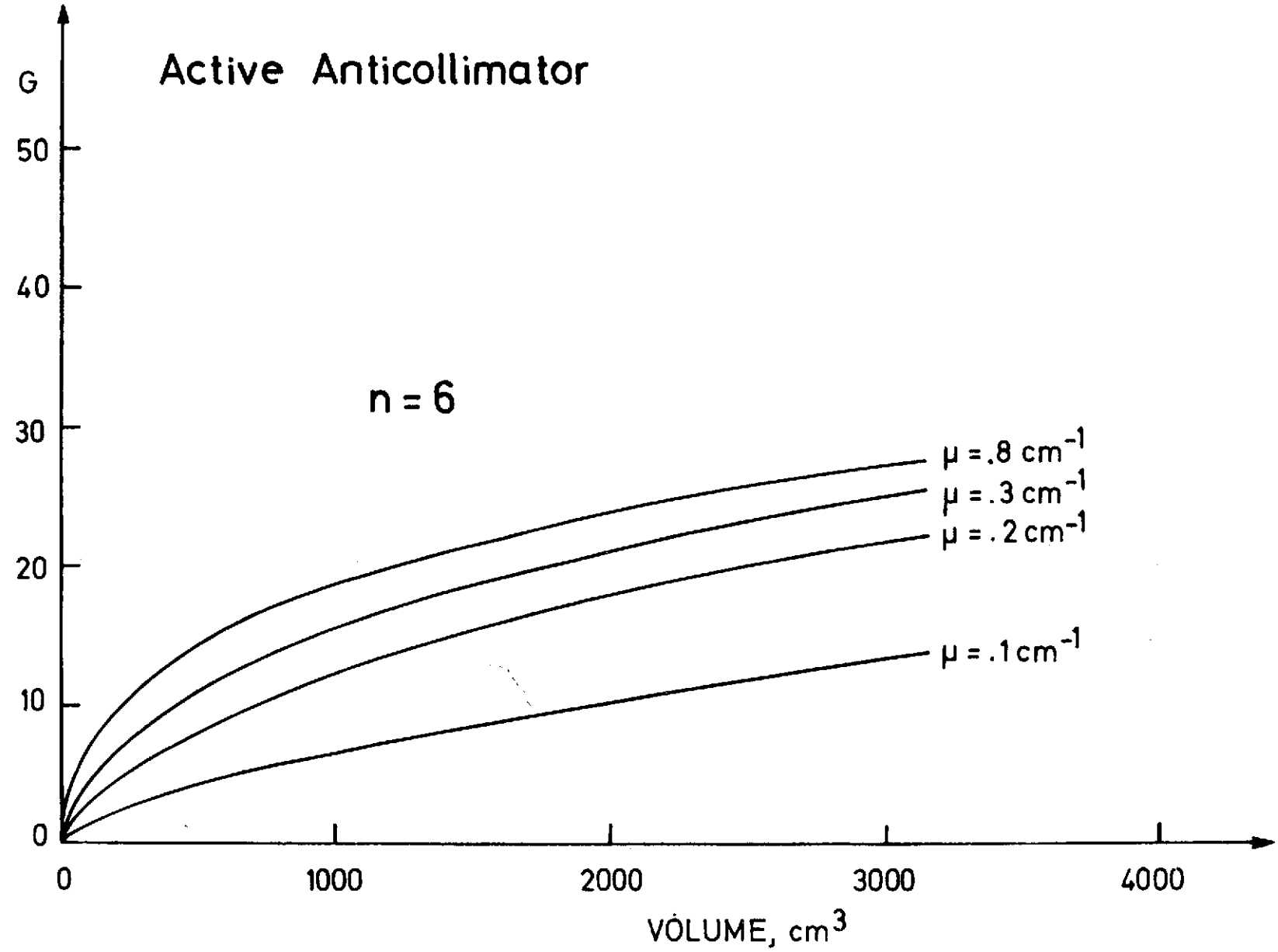
Active Anticollimator
G
50
40
30
20
10
0
n = 6
μ = .8 cm⁻¹
μ = .3 cm⁻¹
μ = .2 cm⁻¹
μ = .1 cm⁻¹
0
1000
2000
3000
4000
VOLUME, cm³

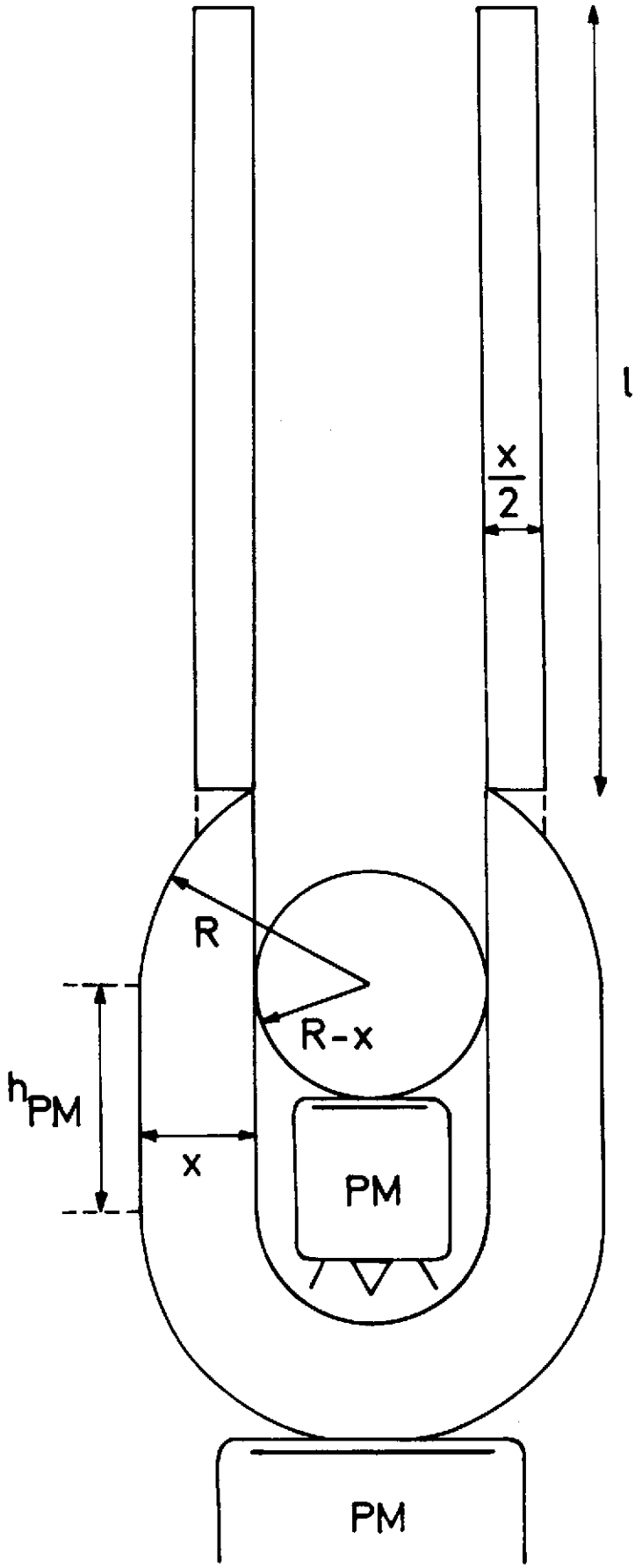
l
x/2
R
R-x
h_PM
x
PM
PM

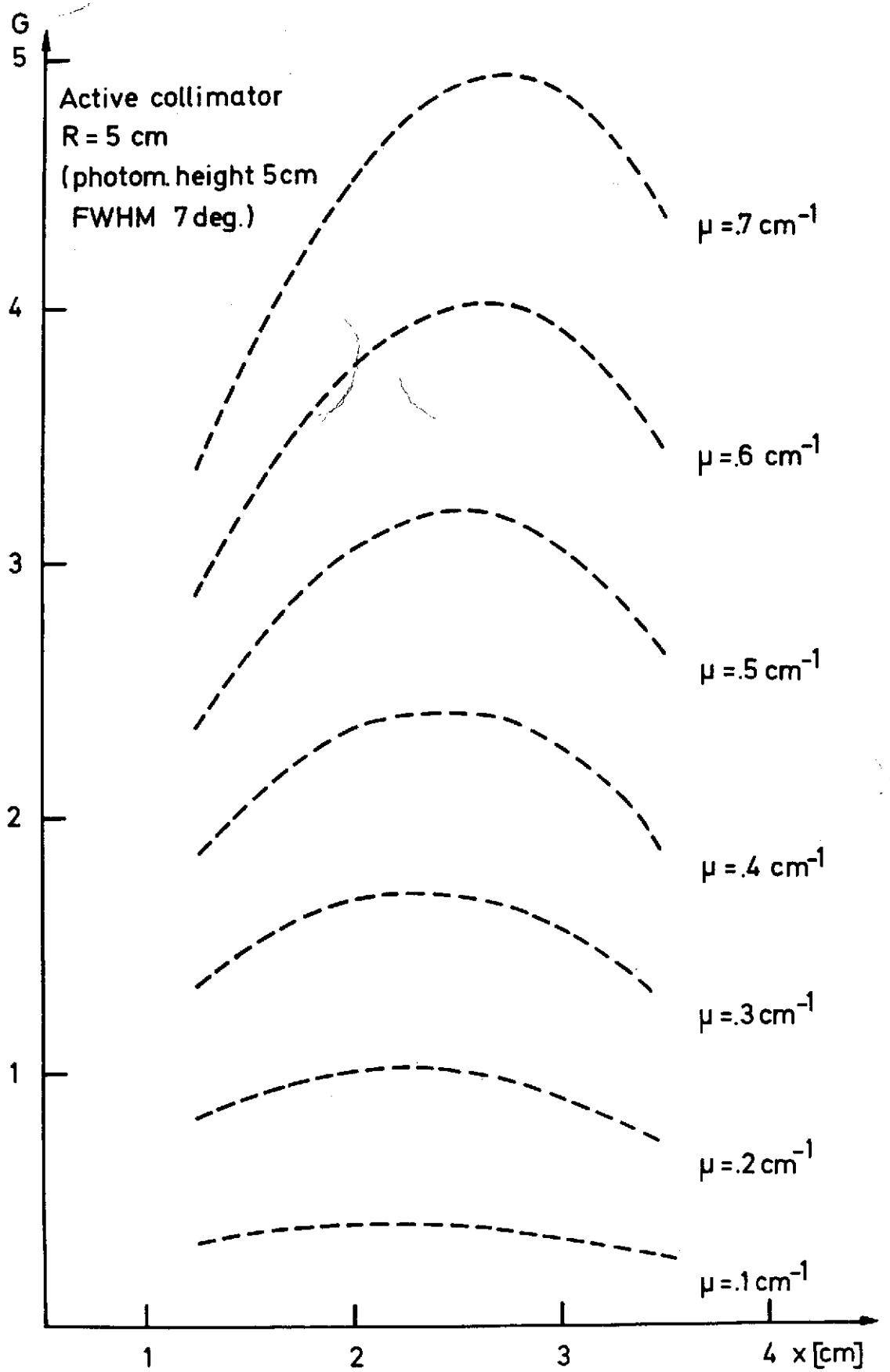
G
5
4
3
2
1
Active collimator
R = 5 cm
(photom. height 5cm
FWHM 7deg.)
μ =.7 cm⁻¹
μ =.6 cm⁻¹
μ =.5 cm⁻¹
μ =.4 cm⁻¹
μ =.3 cm⁻¹
μ =.2 cm⁻¹
μ =.1 cm⁻¹
1
2
3
4 x [cm]

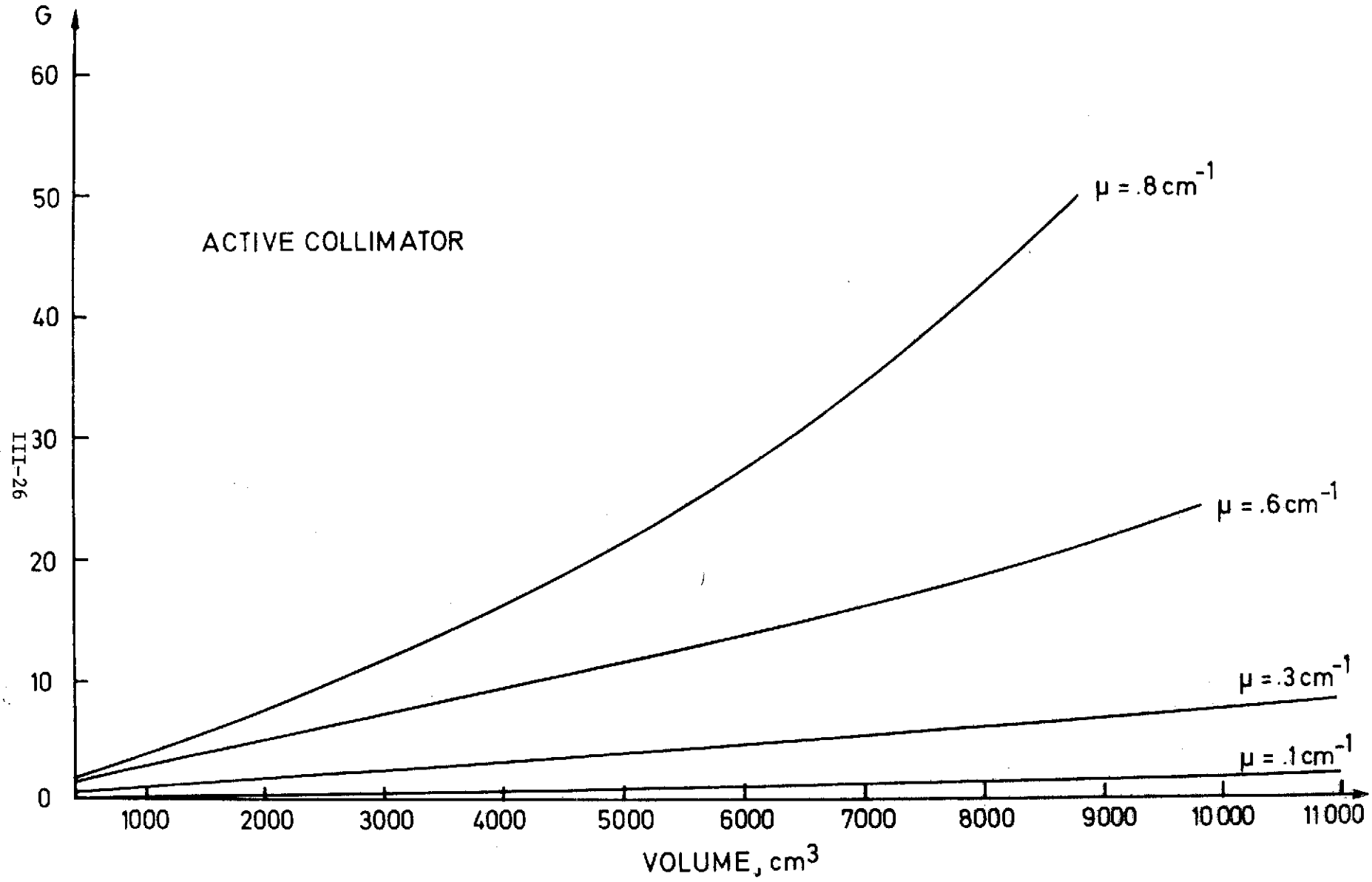
G
60
50
40
30
20
10
0
ACTIVE COLLIMATOR
μ = .8 cm⁻¹
μ = .6 cm⁻¹
μ = .3 cm⁻¹
μ = .1 cm⁻¹
1000
2000
3000
4000
5000
6000
7000
8000
9000
10 000
11 000
VOLUME, cm³

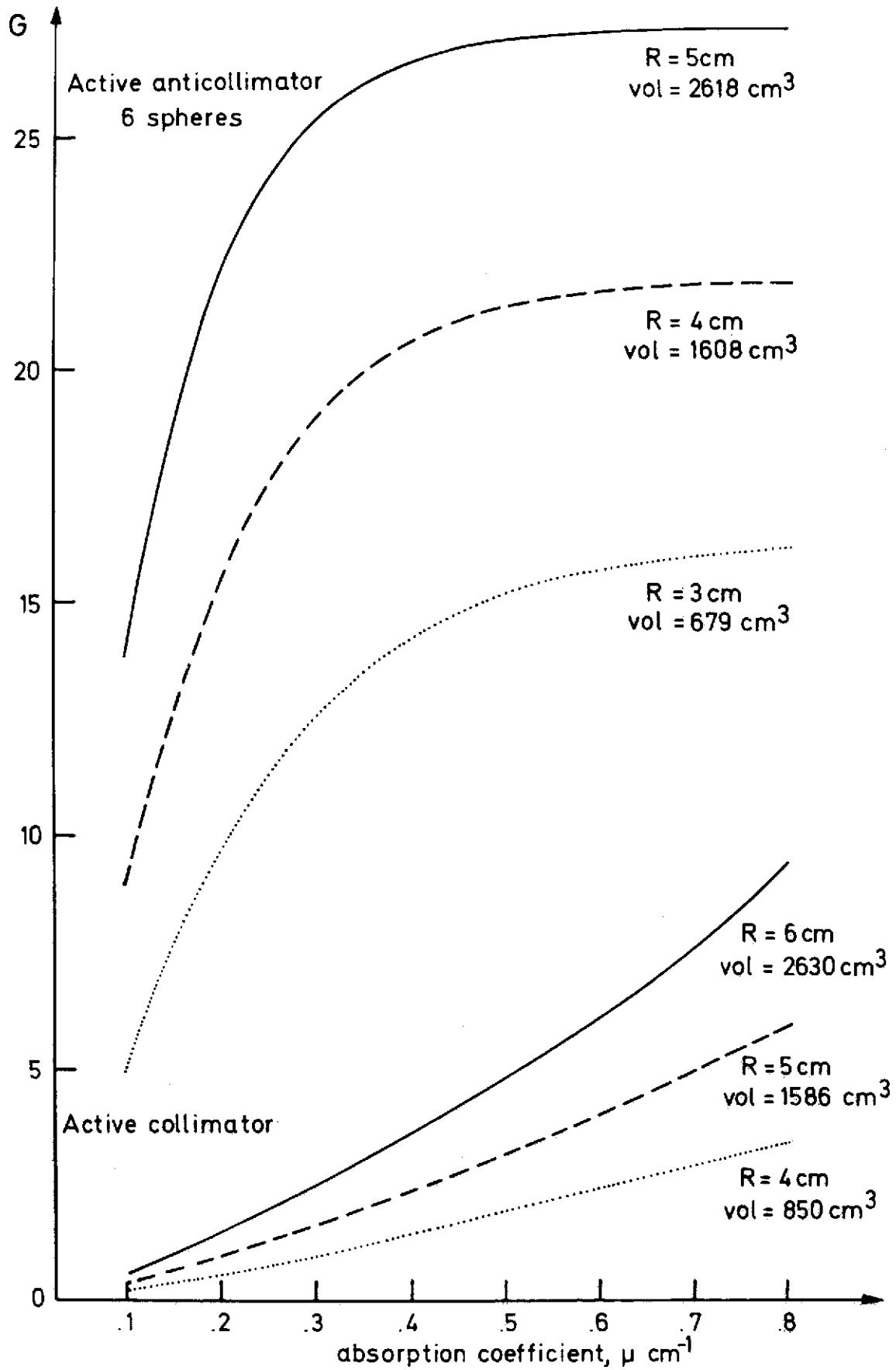
G
Active anticollimator
6 spheres
R = 5cm
vol = 2618 cm3
R = 4 cm
vol = 1608 cm3
R = 3 cm
vol = 679 cm3
R = 6 cm
vol = 2630 cm3
R = 5 cm
vol = 1586 cm3
R = 4 cm
vol = 850 cm3
Active collimator
25
20
15
10
5
0
.1
.2
.3
.4
.5
.6
.7
.8
absorption coefficient, μ cm-1

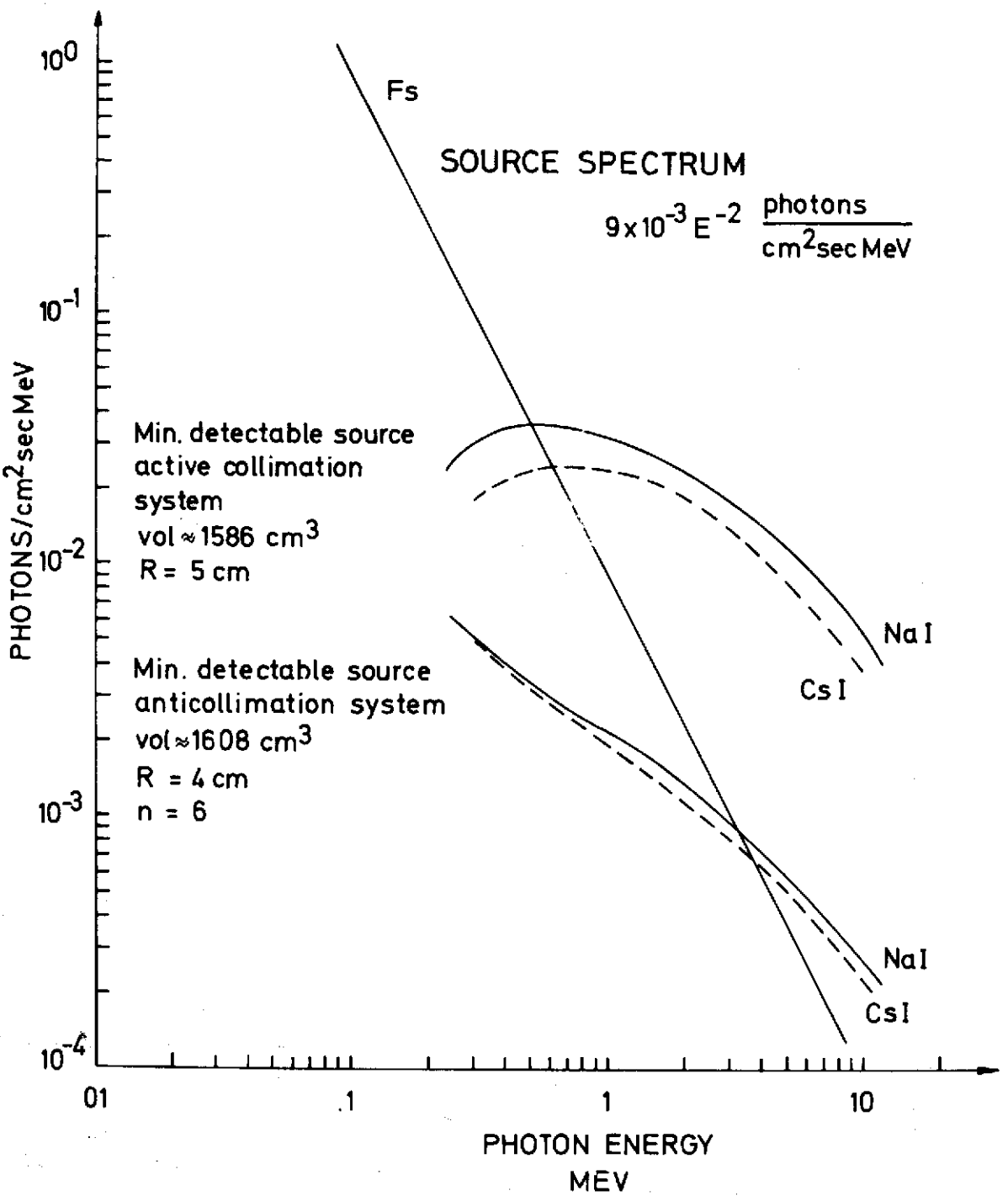
Fs
SOURCE SPECTRUM
$9 \times 10^{-3} E^{-2}$ photons / cm²sec MeV
Min. detectable source
active collimation
system
vol ≈ 1586 cm³
R = 5 cm
Min. detectable source
anticollimation system
vol ≈ 1608 cm³
R = 4 cm
n = 6
NaI
CsI
NaI
CsI
PHOTONS/cm²sec MeV
10^{0}
10^{-1}
10^{-2}
10^{-3}
10^{-4}
01
.1
1
10
PHOTON ENERGY
MEV

N74-11613

ANISOTROPIC DETECTOR SYSTEM FOR THE MEASUREMENT OF GAMMA RAY SOURCE POSITION

by

J. I. Trombka, E. L. Eller, J. I. Vette,
R. L. Schmadebeck and F. W. Stecker

We have been studying the detection efficiencies of cylindrical detectors for various gamma ray photon angular distributions in the energy range from .10 MeV to 15 MeV. It is found that a properly chosen cylindrical crystal can produce a significantly modulated count rate as a function of angle when rotated in the anisotropic flux. These studies further indicate that simple detector systems can be used on small satellites for the determination of a gamma ray source position.

The response of a particular detector can be expressed in terms of a detection efficiency, which depends on the geometry of the system and upon the angular distribution of the incident flux being measured. The details of our calculations can be found in Reference (1). The results are outlined below and extended to examine source resolution angles for a practical sized detector.

We define an effective detector cross sectional area as

$$\eta = \frac{C}{\int_{\Omega} f d\Omega} \tag{1}$$

where C is the total number of photons per unit time and energy which will interact with the detector, f is the photon flux which is differential in angle and energy and Ω is the solid angle subtended by the source with respect to the detector system.

For the case of a right cylindrical scintillation crystal, η has been calculated as a function of rotation. It has been assumed the cylinder is rotated about an axis perpendicular to the axis of symmetry, and that the gamma ray source lies in a plane perpendicular to the axis of rotation. The results indicate that for a given volume a greater count rate modulation can be obtained with a disc shape (i.e. cylinder height less the diameter) than with a rod shape. Figure 1 is a polar plot indicating the modulation expected for a CsI detector 40.6 cm in diameter and 2.54 cm thick for a gamma rays energy of 4 MeV. The angle indicated on the polar plot measures the angle between the source direction and the axis of symmetry. The radial coordinate measures the ratio of $\eta(\theta)$ to $\eta\ (\frac{\pi}{2})$ (i.e. axis of symmetry perpendicular to the source direction.) In this case one obtains a modulation of over four to one. If the source direction makes an angle α with respect to the rotation axis, then the peak of the modulation only reaches the value of $\theta = 90 - \alpha$ on the curve in Figure 1. In the case of such detectors one looks for the minimum instead of the maximum for source location.

To illustrate the angular resolution for sources let us consider the modulated count rate from two gamma ray sources of spectral intensity equal to the Crab nebula ($\sim .009E^{-2}$ photons/cm^2-sec-Mev, Reference 2). This is superimposed on a constant background count rate produced by a diffuse isotropic flux of $.024E^{-1.7}$ photons/cm^2-sec-ster-Mev as measured by Apollo 15 between 0.3 and 30 MeV (Reference 3). For this illustration we use a NaI(Tl) crystal 5.08 cm. thick and 20.32 cm. in

diameter, which is a more realistic size for a small satellite than the one used in Figure 1. The resultant count rates, integrated from 0.3 to 30 MeV, due to the two "Crab" sources and the diffuse background are shown in Figures 2 and 3 for different source positions. The angle b_z' is the angle between the axis of symmetry of the detector and a selected direction in the plane perpendicular to the spin axis. The sources are chosen to lie in this perpendicular plane at angles b_1 and b_2. The average count rates over 3° intervals are shown in Figure 2a for the case $b_1 = 0$ and $b_2 = 180^\circ$. The second derivative of the modulated count rate shown in Figure 2b is obtained using the method os splines. It can be seen that the sharp peak in the second derivative occurs when $b_z' = b \pm 90^\circ$ and because of the double valued response function, the two sources cannot be separated. The modulation for the sources separated by 12° is shown in Figure 3a ($b_1 = +6$, $b_2 = -6$). The second derivative of this modulated count rate is given in Figure 3b and indicates the resolution capability of the detector. The precision of the numbers used in this calculation introduced the irregularities in the second derivative curves. Theoretically, we find that sources separated by 6° or greater should be resolved. In actual practice, signal to background ratio and statistics, as determined by source strength and counting time, respectively,will cause the resolution to be somewhat greater than 6°. Of course to do source locations to these accuracies would require scanning the sky with different spin axis directions since for a signle spin direction a detectable source is only defined to lie on a great circle of the celestial sphere. Additional sources which are detectable will produce

sharp minima as the plane defined by the disc crosses the source. This indicates briefly some of the properties of these systems.

In terms of transient event detection, the rotational period would have to be small compared to the duration of the event. Thus, a satellite rotating at about one revolution per second should allow great circle determination of source position for events lasting 10 seconds or more. Comparison of time of arrival between two satellites with omnidirectional detectors defines a small circle on the celestial sphere on which the source must lie. However, comparison of time of arrival between this type detector and another satellite carrying an omnidirectional detector will confine the source to two directions. Two satellites employing this detector system can define the source location. Thus, in a direction finding sense, this detector system is equivalent to two satellites separated far enough to provide time of arrival comparisons. Consequently in any plans to monitor for burst events by multiple satellites, it would be advantageous if at least one such satellite employed a detector system of this type.

We are presently designing a gamma ray small satellite for studying differential energy distribution for the gamma ray diffuse background and for detecting gamma ray sources (transient or constant) by the method described above. A NaI(Tl) detector of the size illustrated in Figures 2 and 3 will be employed with a charged particle anticoincidence shield. The system will also include charged particle anticoincidence shields around most of the mass of the satellite in order to reduce the back-

ground effects of prompt secondary gamma emission produced by cosmic rays interacting with the satellite material. We believe that such a satellite will be very useful in contributing to a network of detectors used to monitor and study transient gamma ray events.

REFERENCES

1. J. I. Trombka, J. I. Vette, F. W. Stecker, E. L. Eller and W. T. Wildes, "Shaped Scintillation Detector Systems for Measurements of Gamma Flux Anisotropy", NASA X-641-73-230, August 1973.

2. G. H. Shore, "Recent Observations of Cosmic Gamma Rays from 10 MeV to 1 GeV", Proceedings of the International Symposium and Workshop on Gamma Ray Astrophysics, Goddard Space Flight Center preprint, X-641-73-180, June 1973.

3. J. I. Trombka, A. E. Metzger, J. R. Arnold, J. L. Matteson, R. C. Reedy, and L. E. Peterson, Astrophys. J., 181, (1973), 737-746.

FIGURE CAPTIONS

Figure 1. Polar plot of the relative effective detector cross sectional area $\eta(E,\theta)/\eta(E,\pi/2)$ as a function of θ, the angle between the axis of symmetry and the source direction. This is for a CsI crystal 40.62 cm. in diameter and 2.54 cm. thick and for 4 MeV photons.

Figure 2. Integrated count rate and its second derivative for two point sources equal to the Crab Nebula superimposed on the isotropic background as a function of detector orientation. Both sources are at $b = 0^{\circ}$ or 1 source is at $b = 0^{\circ}$ and another at $b = 180^{\circ}$.

Figure 3. Integrated count rate and its second derivative for two point sources equal to the Crab Nebula superimposed on the isotropic background as a function of detector orientation. One source is a $b = -6^{\circ}$ and another is at $b = +6^{\circ}$.

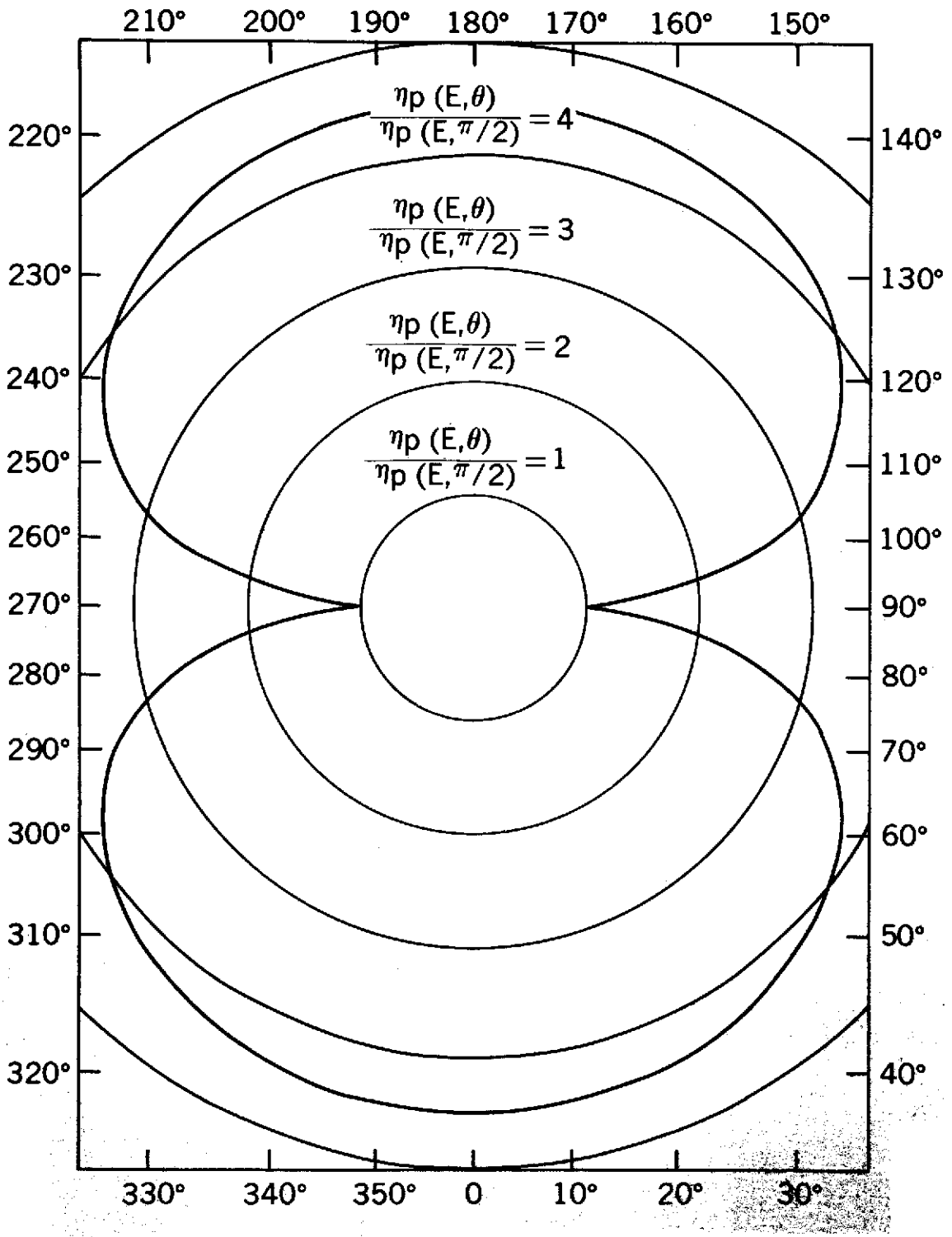
210°
200°
190°
180°
170°
160°
150°
220°
230°
240°
250°
260°
270°
280°
290°
300°
310°
320°
140°
130°
120°
110°
100°
90°
80°
70°
60°
50°
40°
330°
340°
350°
0
10°
20°
30°
$\frac{\eta p\ (E,\theta)}{\eta p\ (E,\pi/2)} = 4$
$\frac{\eta p\ (E,\theta)}{\eta p\ (E,\pi/2)} = 3$
$\frac{\eta p\ (E,\theta)}{\eta p\ (E,\pi/2)} = 2$
$\frac{\eta p\ (E,\theta)}{\eta p\ (E,\pi/2)} = 1$

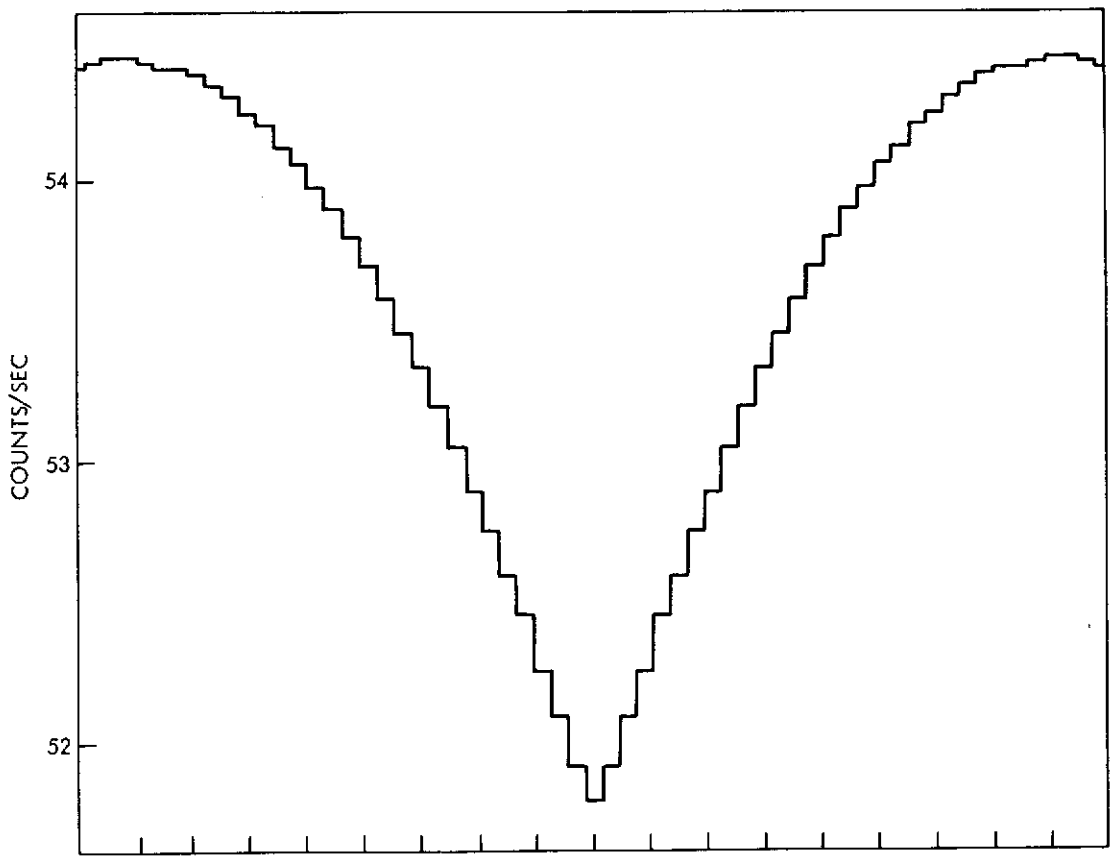

FIGURE 2a

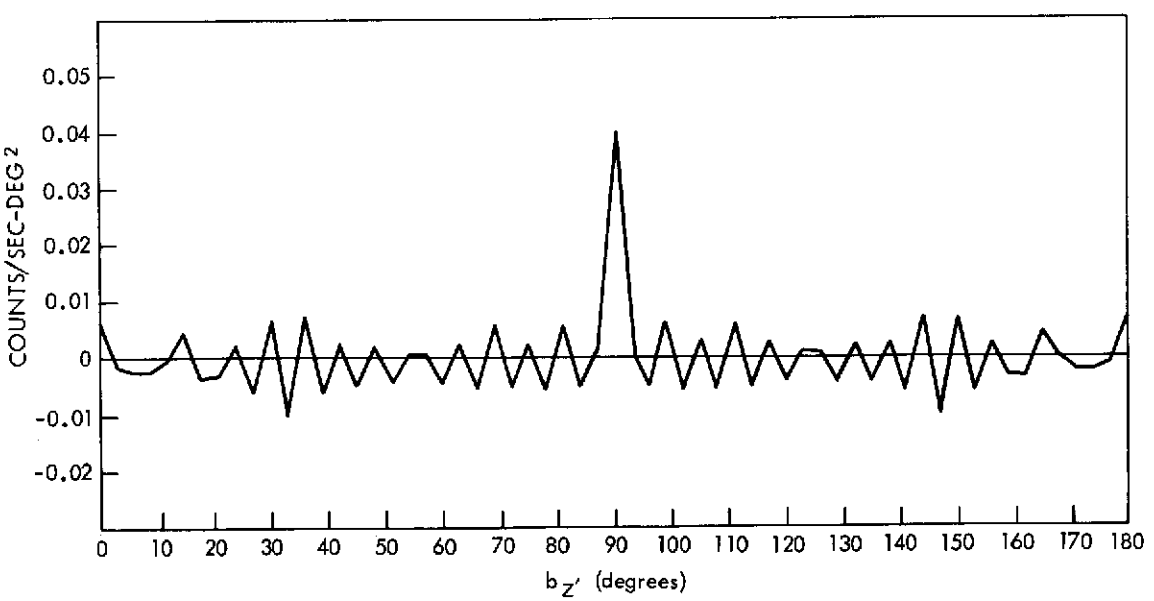

FIGURE 2b

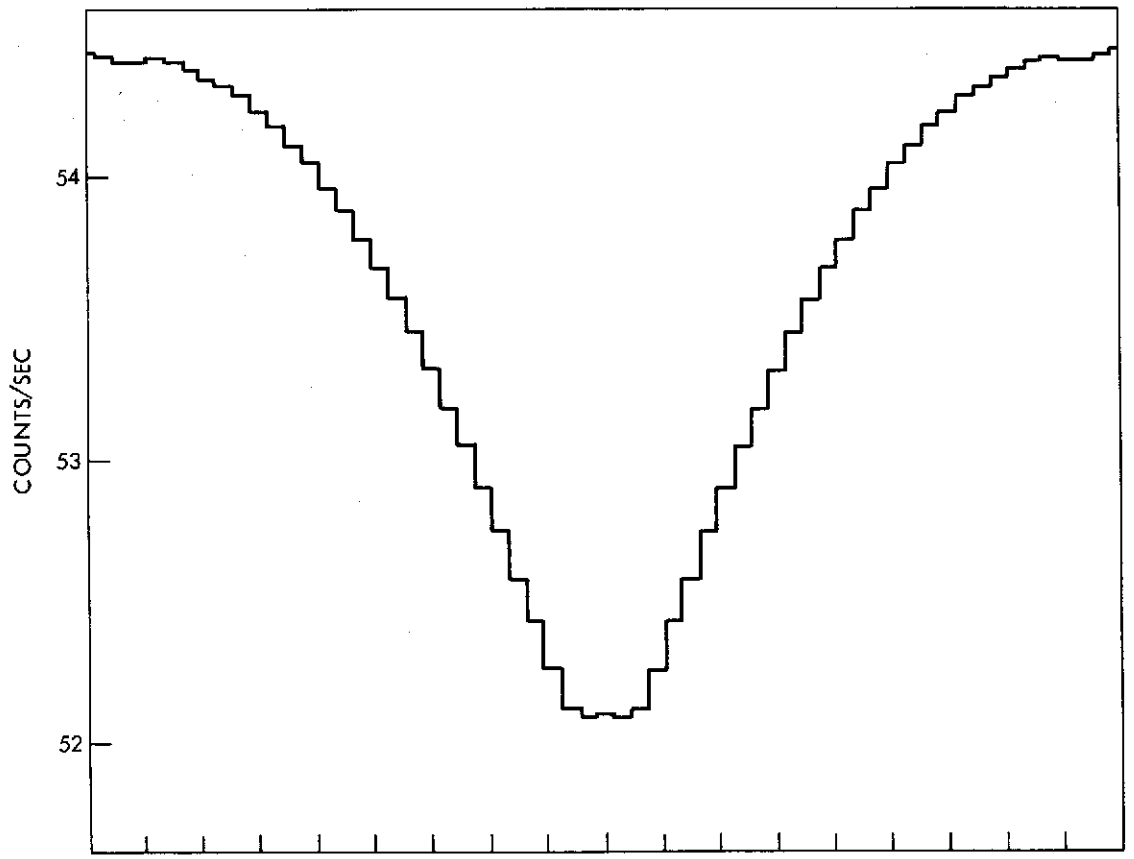

FIGURE 3a

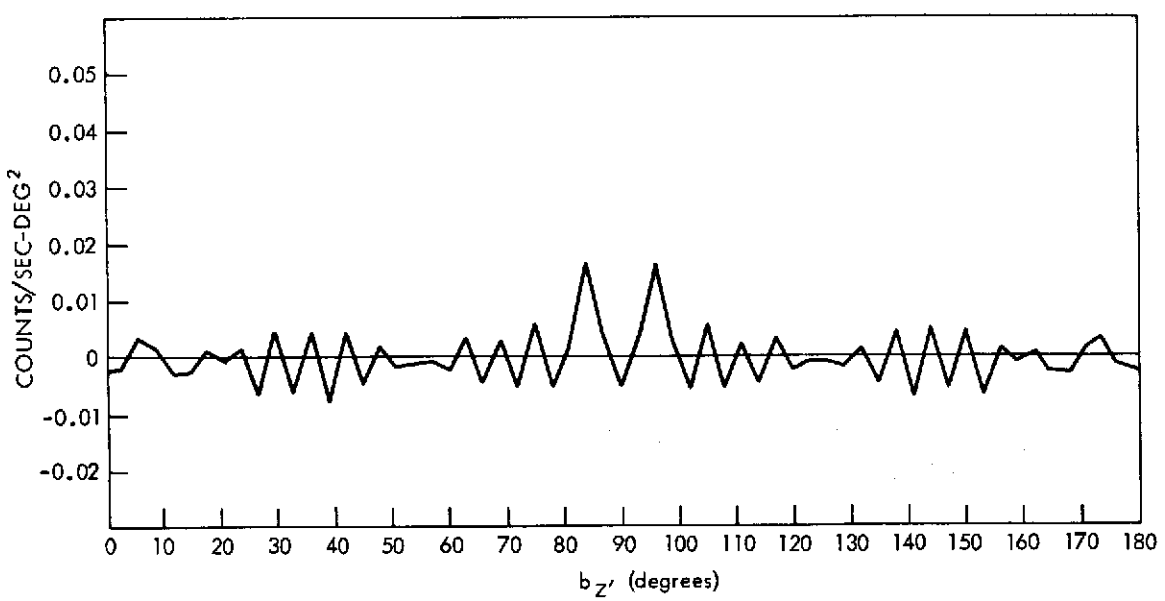

FIGURE 3b

COOLING BLACKBODY: A MECHANISM FOR COSMIC GAMMA-RAY BURSTS

Reuven Ramaty
Goddard Space Flight Center
Greenbelt, Maryland 20771

and

Jeffrey M. Cohen
University of Pennsylvania
Philadelphia, Pennsylvania 19104

A Talk Presented by R. Ramaty at the Los Alamos Conference on Transient Cosmic Gamma- and X-Ray Sources, September 21, 1973.

Abstract

We show that blackbody radiation of variable temperature can account for the observed spectra of cosmic gamma-ray bursts. The temperature variation could be due to cooling by gamma-ray emission. For the model that we consider, an initial temperature of about 2×10^9 °K decreases by a factor of about 3 during the observed duration of the bursts of about 2 seconds. Time integrated blackbody emission can then account for the observed spectrum in the gamma-ray region. When the temperature is further decreased, blackbody emission can also account for the X-ray observations.

Possible sources for the gamma rays could be collapsing white dwarfs. This collapse could be caused by accretion which raises the mass above the Chandrashekhar limit. The gravitational energy released during the collapse causes the emission of neutrinos which heat the surface of the star to the desired temperature. The size of the

radiating region is about 10^6 to $3x10^8$ cm and its distance is between several tenths of megaparsecs to about 100 Mpc. The observed time variations are consistent with large amplitude oscillations of a white dwarf.

N74-11614

We examine blackbody emission as a possible radiation mechanism for cosmic gamma-ray bursts (Klebesadel et al.,1973). The observed photon energy spectra of these bursts in the ~100 keV to ~1 MeV range are of the form

$$\Phi(E) \propto \exp(-E/E_o) \quad , \tag{1}$$

where Φ is measured in photons cm^{-2} keV^{-1}, E is photon energy, and E_o is a parameter which varies from event to event, but is generally in the range from about 100 to 200 keV (Cline et al., 1973). For the one event which was observed in X-ray region as well (14 May, 1972), the spectrum between about 10 keV to 100 keV is a power law of the form E^{-1} (Wheaton et al., 1973).

The photon flux density at earth (in photons $cm^{-2}sec^{-1}keV^{-1}$) from a spherical source of radius r emitting blackbody radiation is

$$\varphi(E) = \frac{2\pi}{c^2h^3}\left(\frac{r}{d}\right)^2 \frac{E^2}{\exp(E/kT) - 1} \tag{2}$$

where T is the temperature and d is the distance to the source. Equation (2), however, cannot be directly compared with the data because the spectral measurements are made over time intervals Δt of the order of the duration of the bursts (~2 seconds), and the temperature is expected to vary over this interval. Instead, the time integral of Equation (2) should be used in this comparison. We therefore evaluate the quantity $\Phi(E)$,

$$\Phi(E) = \int_o^{\Delta t} \varphi(E)dt = \int_{T_o}^{T_1} \varphi(E)\frac{dt}{dT}dT \quad , \tag{3}$$

where $\dot{dT}/dt$ is the rate of change of the blackbody temperature with time, and T_o and T_1 are the initial and final temperatures.

If we assume that

$$\frac{dT}{dt} = - BT^n \tag{4}$$

with B a constant, then

$$\Phi(E) = \frac{2\pi}{c^2 h^3} \left(\frac{r}{d} \right)^2 \frac{k^{n-1}}{B} E^{3-n} \int_{E/kT_o}^{E/kT_1} \frac{x^{n-2} dx}{e^x - 1} \quad . \tag{5}$$

Equation (5) has an interesting limit: for $kT_1 << E << kT_o$, $\Phi(E)$ varies as E^{3-n}. This limit could be applicable to the X-ray region where the observed spectrum is of the form E^{-1}. In our model, this implies that $n = 4$.

A cooling law given by Equation (4) with $n = 4$ is that of an isothermal object losing energy by blackbody radiation. In this case

$$B = \frac{8\pi r^2 \sigma}{3Nk} \quad , \tag{6}$$

where $\sigma = 5.7 \times 10^{-5}$ erg $(°K)^{-4} cm^{-2} sec^{-1}$, and N is the total number of particles involved in the emission. We now proceed to investigate the properties of the source and to compare them with the observations.

By combining Equations (5) and (6) we get

$$\Phi(E) = \frac{3}{4} \frac{k^4}{c^2 h^3 \sigma} \frac{N}{d^2} \frac{1}{E} \int_{E/kT_o}^{E/kT_1} \frac{x^2 \, dx}{e^x - 1} \quad . \tag{7}$$

We can evaluate Equation (7) numerically or via Debye functions (Beattie, 1926). The results are shown in Figure 1 for various values of T_o and T_1.

At high energies ($E > kT_0$), the spectra are straight lines on the semi-logarithmic plot; this means that $\Phi(E)$ is proportional to $\exp[-E/E_0]$ with E_0 close to kT_0. The observed spectra (Cline et al., 1973) then imply that kT_0 is around 100 to 200 keV, or that the initial temperature of the burst is about 2×10^9 °K.

At lower energies ($kT_1 < E < kT_0$) the spectra in Figure 1 are power laws. This power law behavior can be better seen in Figure 2, where the calculated spectra are plotted on a logarithmic plot together with the observed spectrum of the May 14, 1972 burst (Wheaton et al., 1973). For this burst, the kT_0 = 150 keV curve appears to give a very good fit to the observational data.

For blackbody radiation at constant temperature, the data yields not only the temperature but also one relation between the distance and size of the source. This is also the case for a variable-temperature blackbody; however, we have to consider the cooling of the source.

The cooling law, Equation (4) with $n = 4$, gives the time variation of T,

$$T = \frac{T_0}{(1 + t/\tau)^{1/3}} \quad . \tag{8}$$

With B given by Equation (6),

$$\tau = \frac{Nk}{8\pi r^2 \sigma T_0^3} \quad . \tag{9}$$

Because the spectral measurements above 100 keV are made in about 2 seconds (Cline et al., 1973), the blackbody should cool in this time interval from, say, 150 keV to 50 keV. For these parameters,

we get from Equation (8) that $\tau \simeq 0.1$ seconds; then from Equation (9), with $T_o = 2 \times 10^9$ °K, it follows that

$$N \simeq 10^{40} r^2 . \qquad (10)$$

Here, r, the radius of the source is in cm.

Next, we consider the absolute normalization of the calculated flux densities. From Figure 1, for, say, E = 200 keV, kT_o = 150 keV and $kT_1 < 50$ keV, $\Phi = 2 \times 10^{-4}$ Nd^{-2} photons $cm^{-2} keV^{-1}$. This flux density should be compared with an observed flux density at the same energy. For the 14 May, 1972 event, in the first pulse, Φ(200 keV) $\simeq$ 0.2 photons cm^{-2} keV^{-1} (Cline et al., 1973). Therefore, for this event, $N \simeq 10^4 d^2$, where d is in cm. By comparing this result with Equation (10), we get that the distance to the source is given in terms of its radius by

$$d \simeq 10^{18} r . \qquad (11)$$

Before inserting numerical values into Equations (10) and (11), we consider the objects that could produce blackbody radiation in the X-ray and gamma ray regions. In a separate publication (Cohen and Ramaty, 1974), we have discussed collapsing white dwarfs as sources of cosmic gamma-ray bursts. Here we repeat some of this discussion.

When a white dwarf accretes matter (for example, froma binary companion) and its mass exceeds the Chandrashekhar limit it collapses. Since this limit is less than the maximum stable mass of a neutron star, the collapse should proceed to a neutron star. This process releases about 10^{53} ergs of gravitational energy and most of this

energy is carried away by neutrinos. A fraction of the neutrino luminosity, however, is deposited in the neutron star and this could heat the crust to the desired temperature of $\sim 10^9$ °K.

After the collapse, the star may rebound. Cocke and Cohen (1968) have studied the large amplitude pulsations of a degenerate star oscillating between radii of about 10^6 to 3×10^8 cm. These oscillations have periods of a few seconds; hence they could account for the observed time variations of the bursts on the scale of a few seconds (Klebesadel et al., 1973). The large neutrino luminosity, however, will rapidly damp the oscillations and this can explain the transient nature of the bursts as well as the fact that some bursts show single peaks only.

The gamma-ray burst observations also show time variations on a scale of a few tenths of seconds (Klebesadel et al., 1973). These could be due to oscillations of the rebounding star. Because of the radius of the star during rebound is intermediate between the radii of a neutron star and a white dwarf, its oscillation period should also be intermediate between the oscillation periods of such objects. The period of a white dwarf is of the order of a few seconds (Cohen et al., 1969) and the period of a neutron star is about 10^{-3} seconds (Cohen and Cameron, 1971).

We thus assume that $10^6 < r < 3 \times 10^8$ cm. Then, from Equation (10), the total number of particles is in the range 10^{52} to 10^{57}. With $kT_o \simeq 10^{-7}$ erg, this range corresponds to an initial thermal energy of 10^{45} to 10^{50} ergs. Because the total gravitational energy released

during the collapse is $\sim 10^{53}$ ergs, the gamma-ray efficiency is about 10^{-8} to 10^{-3}.

For the same range of r, the distance to the source is 10^{24} cm<d< 3×10^{26} cm. Thus, if the gamma-ray bursts are produced by blackbody radiation, their sources should be extragalactic because the lower limit on d is greater than any galactic dimension. (For the sources to be galactic, r has to be about 1 meter, an unlikely size for a 10^{9} °K blackbody.)

The upper limit on d (~100Mpc) is greater than the distance to the Virgo cluster (~ 10Mpc, Allen 1963). Most of the galaxies within a distance of about 10 Mpc from our own are in the Virgo cluster (ℓ^{II} = 284°, b^{II} = 74°); thus, the fact that there is no anisotropy in arrival directions of the gamma-ray bursts means that the sources of the majority of the bursts are either much closer or much farther than about 10 Mpc.

References

Allen, C. W. 1963, Astrophysical Quantities (Athlone Press, London).

Beattie, J. A. 1926, J. Math. Phys., 6, 1.

Cline, T. L., Desai, U. D., Klebesadel, R. W. and Strong, J. B. 1973, Astrophys. J. Letters, in press.

Cocke, W. J. and Cohen, Jeffrey M. 1968, Nature, 219, 1009.

Cohen, Jeffrey M. and Ramaty, R. 1974, Gamma Ray Burst During Neutron Star Formation (to be published).

Cohen, Jeffrey M., and Cameron, A.G.W. 1971, Astrophysics and Space Science, 10, 227.

Cohen, Jeffrey M., Lapidus, A. and Cameron, A.G.W., Astrophysics and Space Science, 5, 113.

Wheaton, Wm. A., Ulmer, M. P., Baity, W. A., Datlowe, D. W., Elcan, M. J., Peterson, L. E., Klebesadel, R. W., Strong, I. B., Cline, T. L. and Desai, U. D. 1973, Astrophys. J. Letters (in press).

Figure Captions

1. Coqling blackbody spectrum. T_o and T_1 are the initial and final temperatures, respectively, N is the total number of isothermal particles involved in the radiation, d is the distance to the source, and $k^4 c^{-2} h^{-3} \sigma^{-1} = 0.024$.

2. Cooling blackbody spectrum and measurements for the May 14, 1972 event. The calculations are normalized to the data.

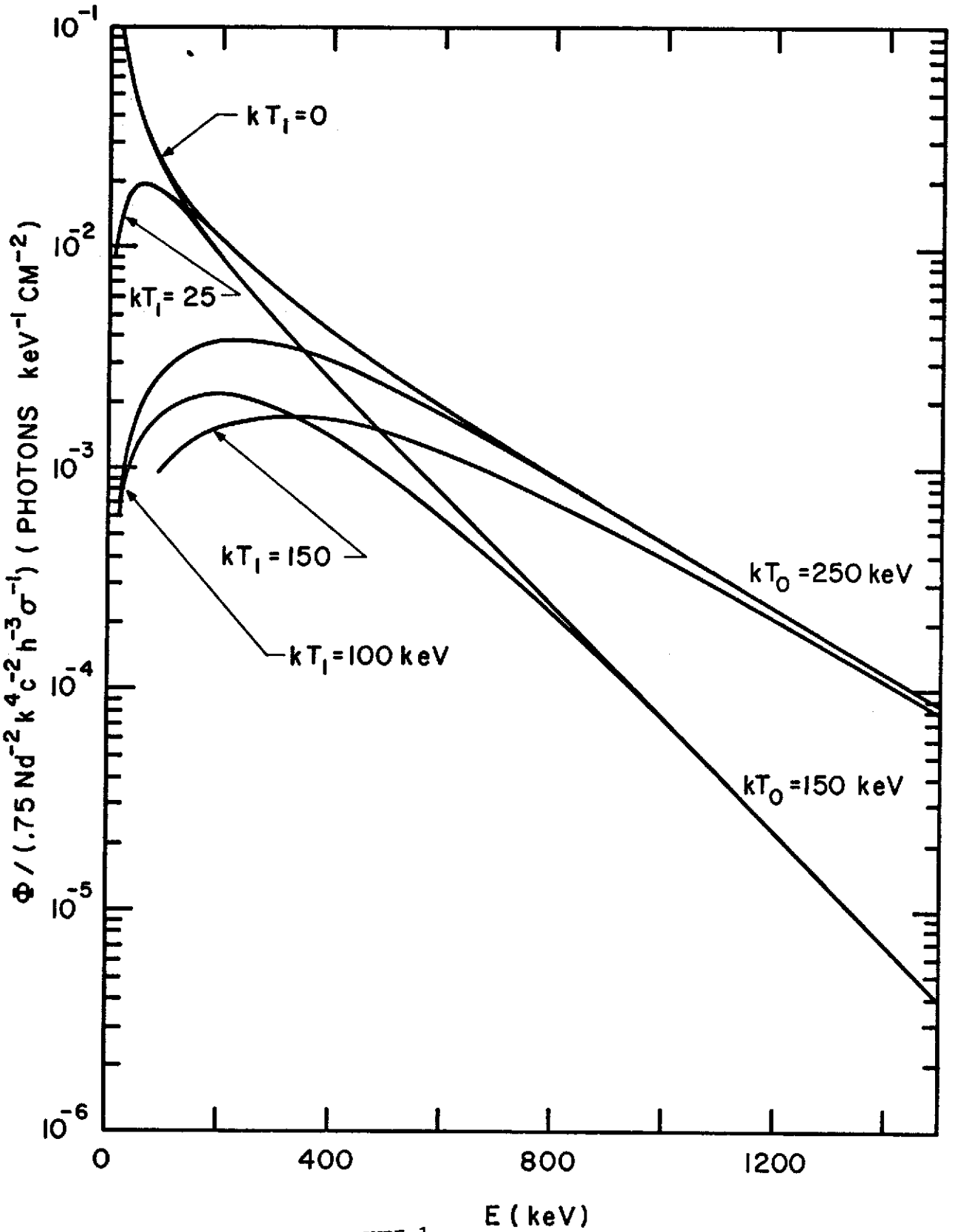
10^{-1}
10^{-2}
10^{-3}
10^{-4}
10^{-5}
10^{-6}
$\Phi / (.75\, Nd^{-2} k^4 c^{-2} h^{-3} \sigma^{-1})$ (PHOTONS keV^{-1} CM^{-2})
kT$_I$=0
kT$_I$= 25
kT$_I$ = 150
kT$_I$=100 keV
kT$_O$ =250 keV
kT$_O$ =150 keV
0
400
800
1200
E (keV)

FIGURE 1

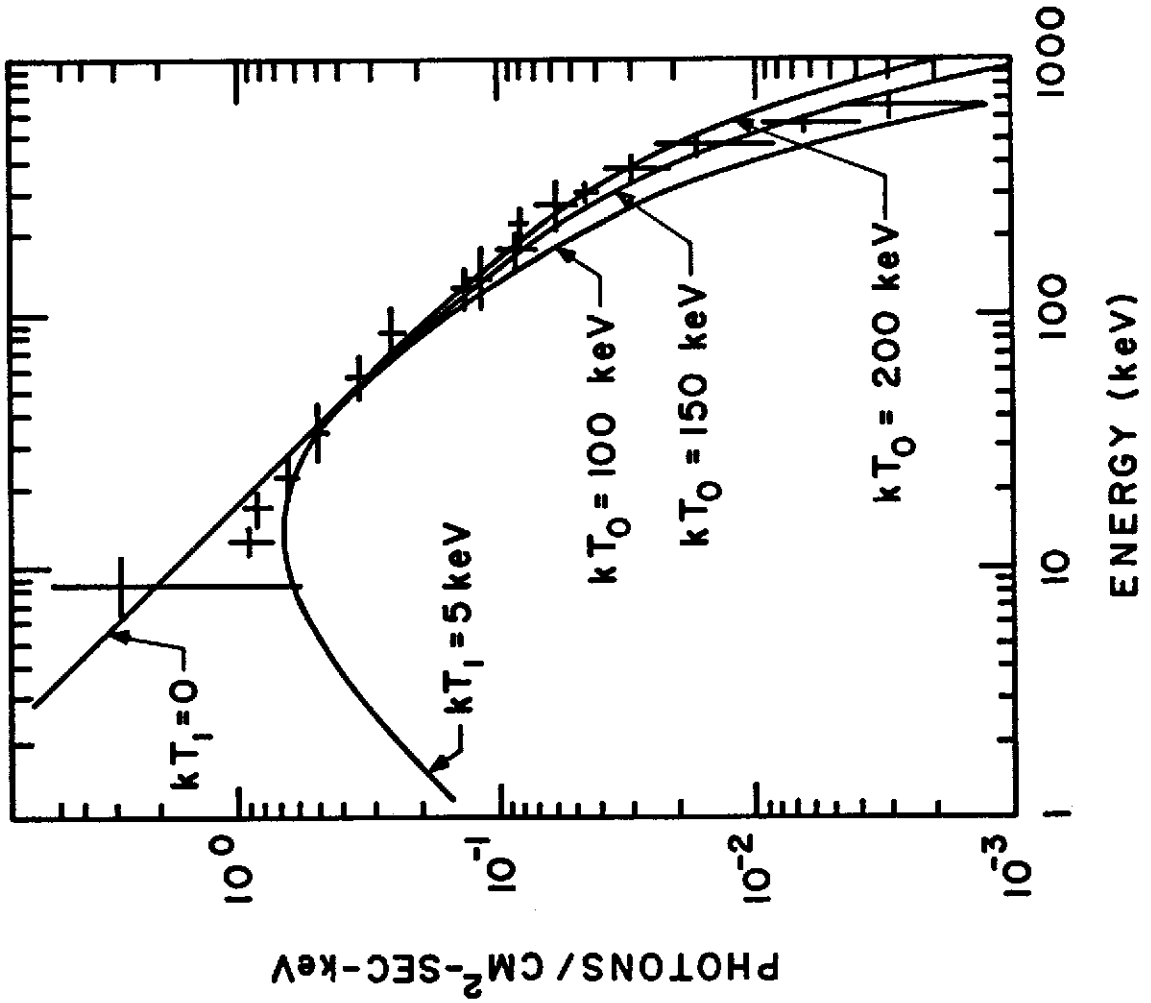
PHOTONS/CM²-SEC-keV
ENERGY (keV)
kT₀ = 100 keV
kT₀ = 150 keV
kT₀ = 200 keV
kT₁ = 5 keV
kT₁ = 0

FIGURE 2

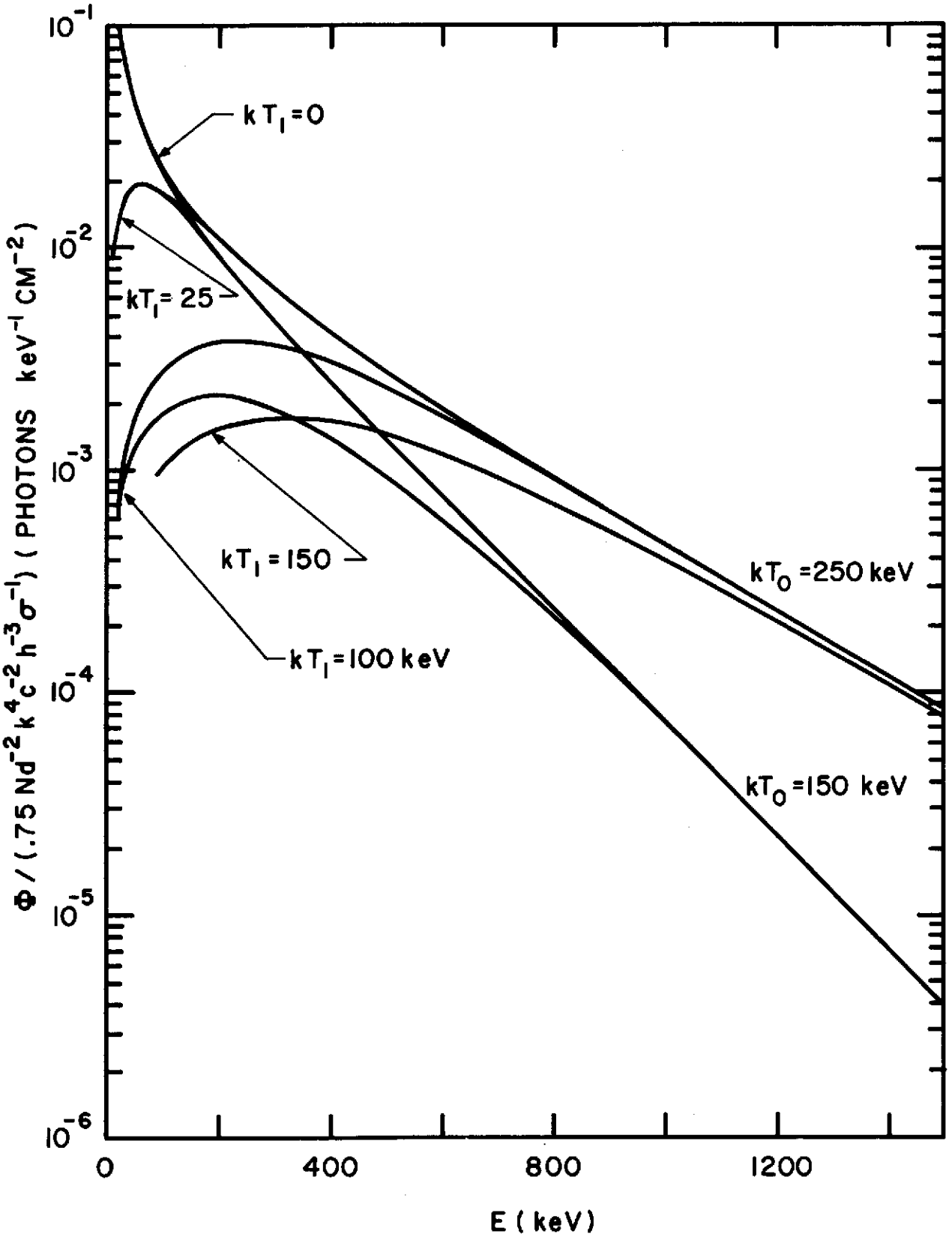
10^{-1}
10^{-2}
10^{-3}
10^{-4}
10^{-5}
10^{-6}
$\Phi / (.75\, Nd^{-2} k^4 c^{-2} h^{-3} \sigma^{-1})$ (PHOTONS keV^{-1} CM^{-2})
$kT_1 = 0$
$kT_1 = 25$
$kT_1 = 150$
$kT_1 = 100$ keV
$kT_0 = 250$ keV
$kT_0 = 150$ keV
0
400
800
1200
E (keV)

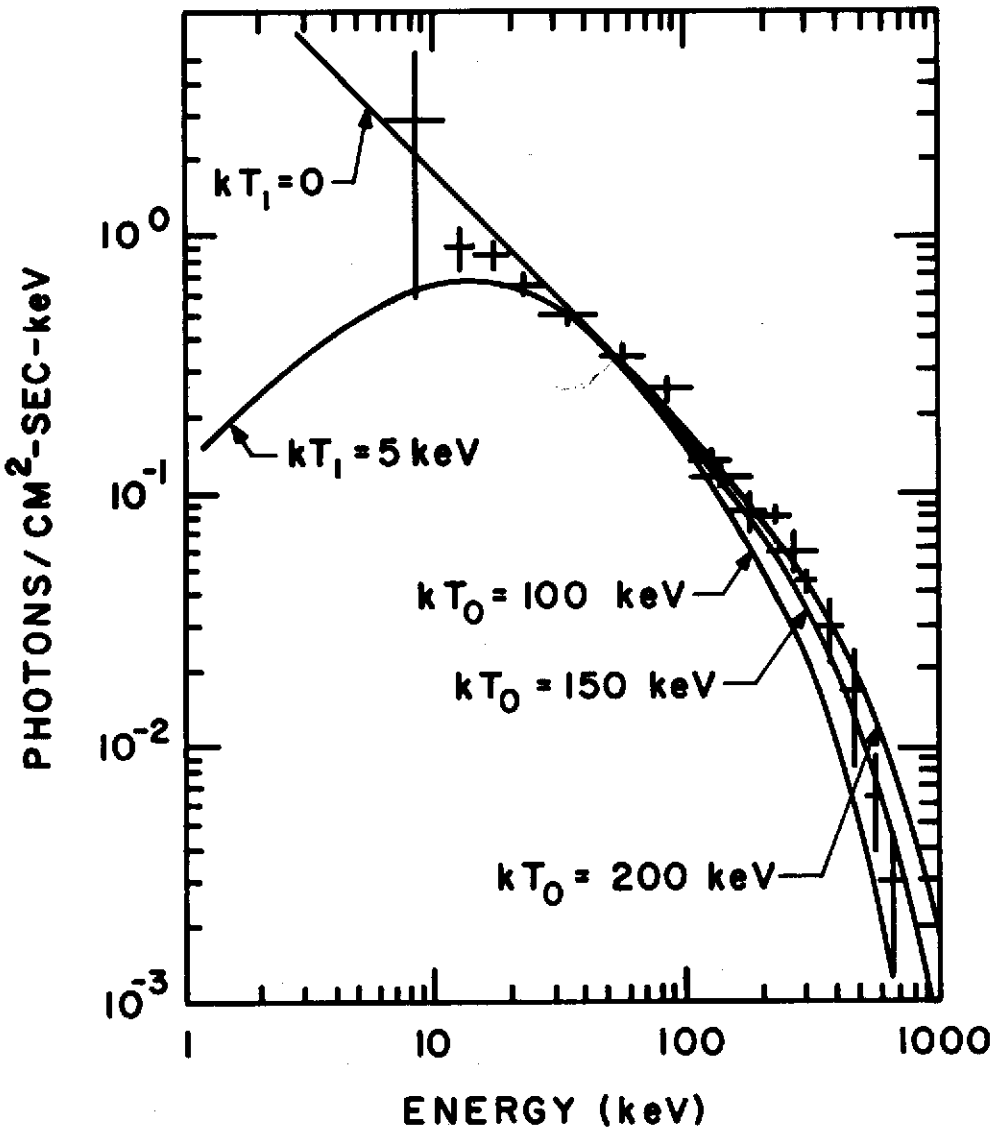
kT1=0
kT1=5 keV
kT0=100 keV
kT0=150 keV
kT0=200 keV
PHOTONS/CM2-SEC-keV
10^0
10^-1
10^-2
10^-3
1
10
100
1000
ENERGY (keV)

COSMIC SOFT GAMMA-RAY BURSTS AND THE STELLAR SUPER-FLARE HYPOTHESIS*

F.W. Stecker

and

K.J. Frost

Goddard Space Flight Center
Greenbelt, Maryland 20771

*Contribution to the Los Alamos Conference on Transient Cosmic Gamma-Ray and X-ray Sources, September 20-21, 1973.

Recently, Klebesadel, Strong, and Olsen (1973) reported the exciting discovery of γ-ray bursts having a typical duration of the order of seconds and typical photon energies of the order of hundreds of keV. This observation has now been confirmed by Cline, Desai, Klebesadel, and Strong (1973) using the detector aboard the satellite IMP-6. This contribution is an expanded version of our previously published paper (Stecker and Frost 1973) suggesting a stellar superflare origin for these bursts.

Predictions of γ-ray bursts from supernovae have been made by Colgate (1968), but there are several difficulties in interpreting the observed bursts as originating in supernovae. In particular, the observed bursts have typical durations of the order of seconds with multiple bursts being common. They also appear to have soft exponential spectra with photon energies in the range of 150 to 250 keV. They have been observed to occur frequently with no apparent correlation with observed supernova events.

In contrast to the observed events, Colgate (1968) has predicted that γ-ray bursts from supernovae would have durations of the order of 10^{-5} s and hard power-law energy spectra with a characteristic energy of about 2 GeV. No correlation has been found between the observed bursts and observed extragalactic supernovae (Klebesadel et al.) and

the supernovae theory does not lead to a straight-forward explanation of multiple bursts. It thus appears to us probable that the observed bursts do not originate in supernovae, and that alternative possibilities for the origin of these bursts should be explored. We discuss here the alternative possibility that these outbursts are simply giant versions of the X-ray bursts typically seen in solar flares.

The observed γ-ray bursts bear a strong resemblance in many respects to the solar X-ray bursts observed recently with a 2-s time resolution (Frost, 1969; Kane, 1969). Figure 1 shows a representative nonthermal solar X-ray burst. This burst is dominated by two impulsive spikes, each about 10 s in duration. If a burst such as this were emitted by a star other than the sun, then only the narrowest parts of the burst might be detected above the background noise. Such bursts would appear to be shorter than solar bursts as is the case with the recently observed non-solar bursts. Thus there may be little intrinsic difference between the time-scales of solar bursts and the suggested stellar bursts at the source. In both cases, the time scale is much longer than that predicted for supernovae. The burst shown in Figure 2 is a single spike of less than 6 s duration.

N74-11615

The spectral characteristics of the nonsolar bursts have been measured by Cline et al. (1973). These spectral data from IMP-6 are found to be well described by an exponential spectrum of the form $I \propto e^{-E/E_o}$ with E_o being between 150 and 250 keV for a typical initial burst. Subsequent bursts in multiple-burst events appear to be softer with $E_o \sim$ 100 keV. The spike component of solar X-ray bursts could also fit an exponential energy spectrum with $E_o \sim 100$ keV (Frost, 1969). Although most solar bursts probably have an E_o somewhat less than 100 keV (but greater than 10 keV), we do not consider this a significant qualitative difference. The multiple spike characteristics seen in the nonsolar bursts are commonly seen in solar X-ray bursts as well.

We therefore consider it generally plausible that these bursts are caused by the bremsstrahlung of electrons accelerated to high energies in a stellar flare event. Assuming the acceleration to depend only on the strength of the effective field seen by the electrons, and not on electron energy, the final energy of the electron will be determined by the time the electron spends in the field. If we assume this acceleration time to be collisionally determined, the average time being T, the probability (P) of an electron being accelerated for time (t) is given by the distribution

$$dP/dt = T^{-1} e^{-t/T} \qquad (1)$$

The spectrum of accelerated electrons would then be of the form

$$I(E)dE \propto (dE/E_o)e^{-E/E_o} \qquad (2)$$

where the mean acceleration rate is given by the constant E_o/T and E_o is the average electron energy. The resulting photon spectrum should then also approximate an exponential form. The above considerations are fairly general and it appears that they may be applicable to both solar and non-solar bursts.

We conclude that the time scale, mean photon energy, and energy spectrum shape (therefore possibly the acceleration mechanism) for both the solar and nonsolar bursts are strikingly similar. There is so much similarity that it is a bit surprising considering that there is such a wide variation of surface conditions among the various stars in the galaxy. There does however appear to be one important difference. The nonsolar bursts that have been observed, which presumably must be both the closest and strongest of the nonsolar bursts, have a much greater intrinsic intensity than their solar counterparts. The strongest solar flares could have a total energy of $\sim 10^{32}$ erg (Bruzek, 1967). The bursts seen by Klebesadel et al. (1973) involve an energy flux of $\sim 10^{-5}$-10^{-4} erg/cm^2. Denoting this flux by ε, the X-ray energy at the source is given by

$$\mathcal{E} \simeq 2\pi R^2 \varepsilon \qquad (3)$$

assuming the source flare radiates into 2π sr. Assuming $\varepsilon \simeq 3 \times 10^{-5}$ erg/cm^2, a source at a distance R = 10 pc would have a typical total X-ray energy $\mathcal{E} \simeq 2 \times 10^{35}$ erg and a corresponding total energy of 10^{38} to 10^{39} erg. A stellar burst of the type hypothesized here would then involve the acceleration of $\sim 10^6$ to 10^7 times more electrons than a strong solar flare. We may speculate that such an event might involve a star with a magnetic field strength $\sim 10^3$ times larger than the sun. Such fields may not be uncommon, particularly in stars earlier than F0, although the observational establishment of these fields is difficult and often impossible (Babcock, 1960). In addition, common white dwarf stars may have surface fields up to 3×10^7 G (Ostriker, 1970) so that they may be likely sources for these bursts. It seems reasonable to assume that such stars as are likely to produce the observed bursts should be near enough so that no concentration toward the galactic plane should be expected.

For example, the density of white dwarfs in the solar neighborhood is $\sim 5 \times 10^{-3}$ pc^{-3}. The Los Alamos group has observed 20 events over a 4 year period (Strong, et al. 1973) for a mean rate of 5 yr^{-1} or 2.5×10^{-4} events per white dwarf per year within 100 pc. The implication is that even

a small fraction of nearby white dwarfs with high magnetic fields and pathological surface conditions might account for the observed events. It seems to us also more likely that white dwarfs with high magnetic fields could produce a larger ratio of X-ray to optical flaring than other stars. Brecher and Morrison (1973) have suggested flaring in F stars, however, it is our opinion that F stars do not differ enough from our sun (similar magnetic fields and $\lesssim$ 6 times solar luminosity) to account for the overall large energy difference between solar and non-solar events.

Strong et al. (1973) have found 6 times as many bursts in the general direction away from the galactic center as towards the galactic center. Since the sun is on the inside of a spiral arm, Strong et al. (1973) argue that this evidence tends to support stellar origin within the galaxy in our local arm within $\sim$ 100 pc of the sun. We thus tend to favor origin of the bursts in population I white dwarfs although we feel that other suggestions presented at this conference, such as those of Brecher and Morrison (1973) and Ramaty and Cohen (1973) are also interesting possibilities. We do not, however, feel that an extragalactic supernova origin for most of the reported events seems likely.

The stellar flare hypothesis immediately lends itself to various observational tests. Possible observational

consequences are: (1) repetitions of the bursts at the same position; (2) possible simultaneous radio bursts at the same position; (However, since we are considering here compact objects with very high magnetic fields, synchrotron self-absorption may eliminate this possibility.), and (3) γ-ray lines at 0.51 MeV (positron annihilation), 2.23 MeV ($n+p \rightarrow d+\gamma$), 4.4 MeV (C^{12*}) and 6.1 MeV (O^{16*}) as have been seen in strong solar flares (Chupp et al., 1973, see also Chapter VI.A). These lines may be present because the flare can accelerate protons as well as electrons so that various nuclear reactions may occur in the flare.

If the stellar flare hypothesis is verified, it may imply a significant source of low-energy cosmic-rays in the solar neighborhood (and throughout the galaxy), depending on the frequency and intensity of the flares.

The authors wish to thank Drs. T. Cline and R. Ramaty for valuable discussions and T. Cline for communicating his data to us prior to publication.

FIGURE CAPTIONS

Figure 1. A multiple solar X-ray burst observed on OSO-5 with a time structure similar to that observed for non-solar bursts.

Figure 2. A single solar X-ray burst also observed by OSO-5. This burst had a duration of less than 6 s.

REFERENCES

Babcock, H.W., 1960, Stars and Stellar Systems, IV, Univ. of Chicago Press, Chicago.

Brecher, K. and Morrison, P., 1973, this conference.

Bruzek, A., 1967, Solar Physics, J. Xanthakis, ed., Interscience Pub. Co., London.

Chupp, E.L., D.J. Forrest, P.R. Higbie, A.N. Suri, C. Tsai, and P.P. Dunphy, 1973, Nature, 241, p.33.

Cline, T.L., V.D. Desai, R.W. Klebesadel, and I.B. Strong, 1973, Astrophys. J. Letters, 185, L1.

Colgate, S.A., 1968, Can. J. Phys. 46, p. S476.

Frost, K.J., 1969, Astrophys. J. Letters, 158, p. L159.

Kane, S.R., 1969, Astrophys. J. Letters, 157, p. L139.

Klebesadel, R.W., I.B. Strong, and R.A. Olsen, 1973, Astrophys. J. Letters, 182, p. L85.

Ostriker, J.P., 1970, Acta Phys., 29, Suppl. 1, p. 69.

Ramaty, R. and Cohen, J.M., 1973, this conference.

Stecker, F.W. and Frost, K.J., 1973, Nature Phys. Sci., October 1, 1973.

Strong, I.B., Klebesadel, R.W. and Olsen, R.A., 1973, this conference, also Bull. Amer. Astr. Soc., in press.

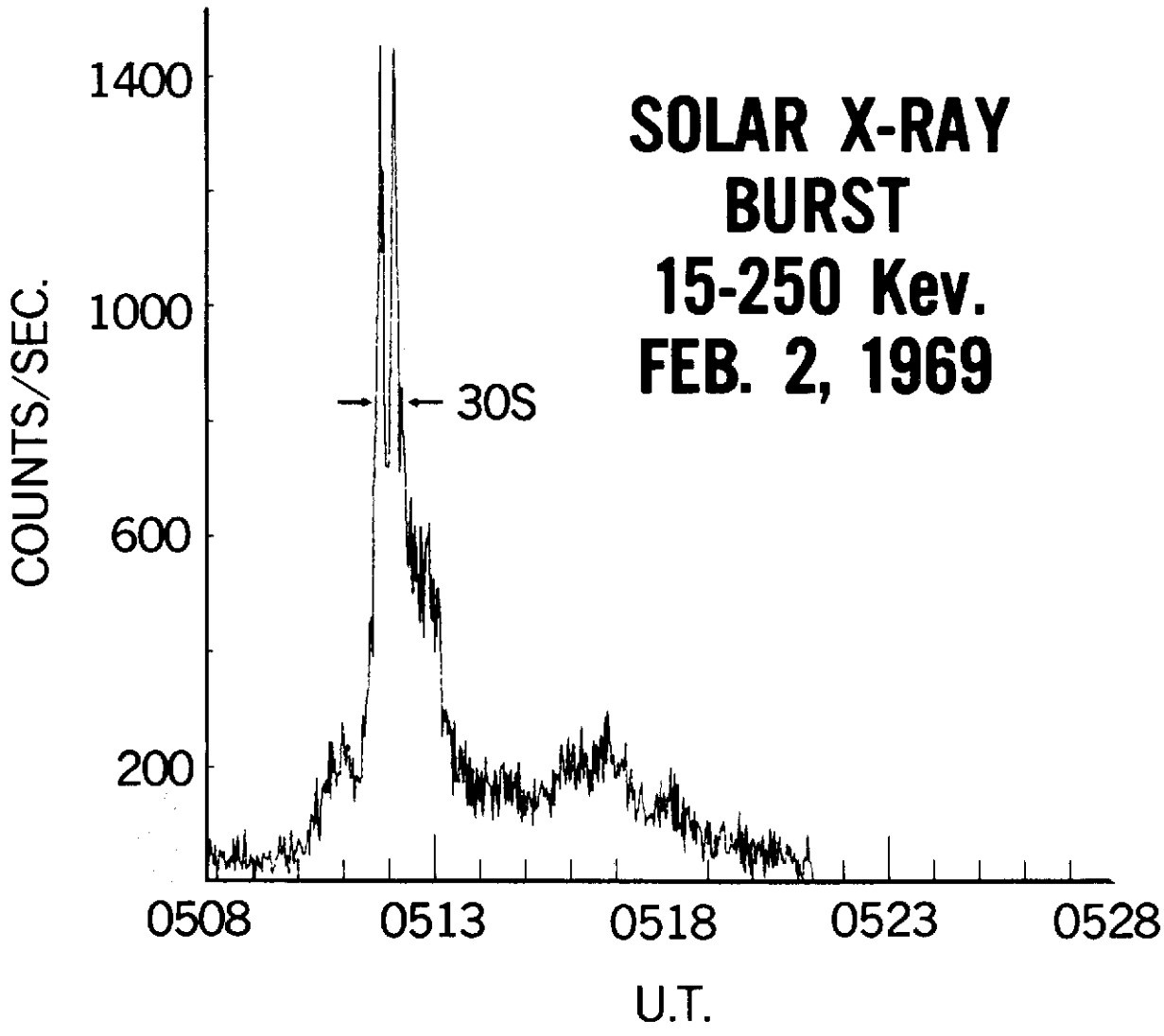
SOLAR X-RAY
BURST
15-250 Kev.
FEB. 2, 1969
30S
COUNTS/SEC.
1400
1000
600
200
0508
0513
0518
0523
0528
U.T.

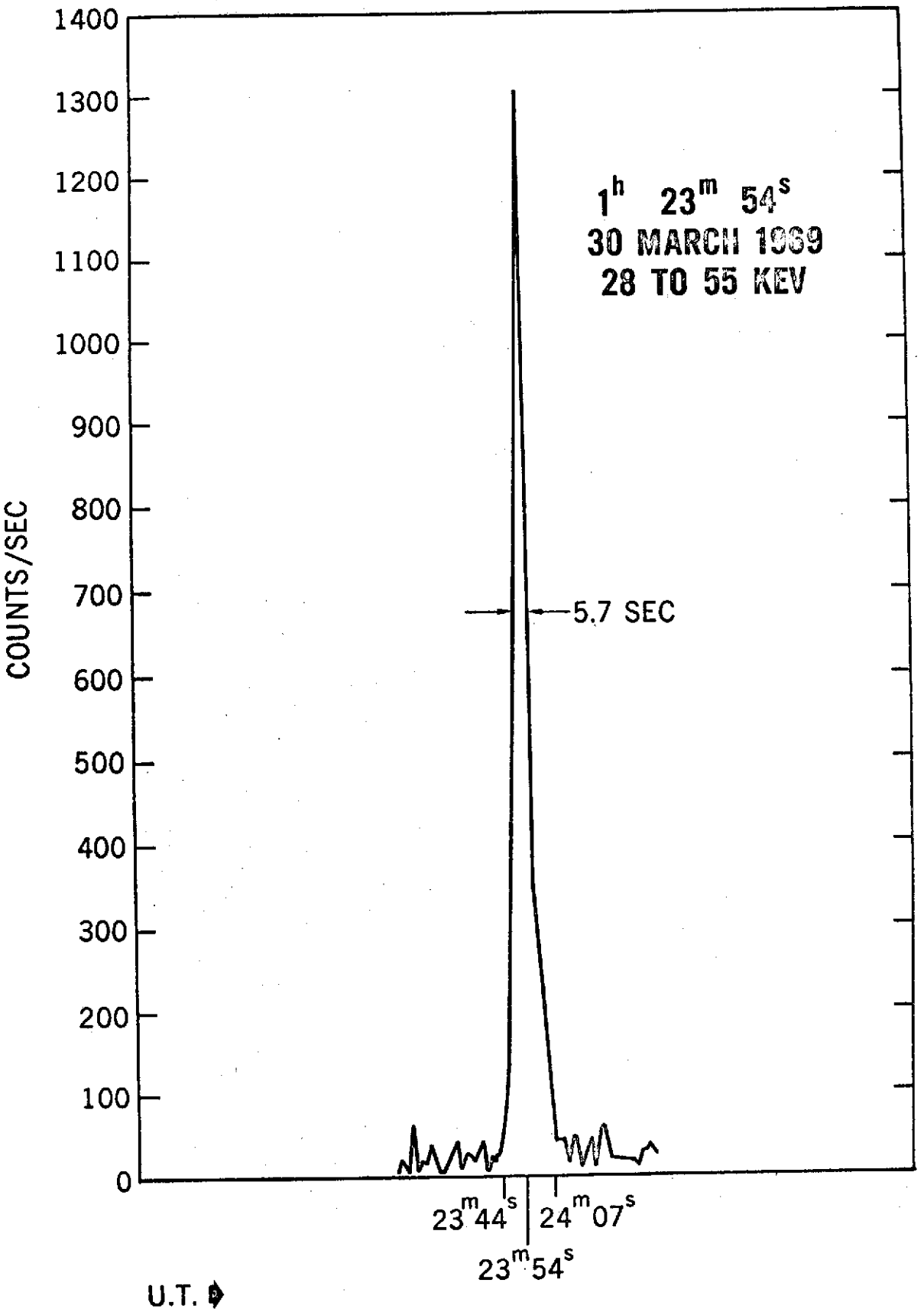
1400
1300
1200
1100
1000
900
800
700
600
500
400
300
200
100
0
COUNTS/SEC
1h 23m 54s
30 MARCH 1969
28 TO 55 KEV
5.7 SEC
23m44s
24m07s
23m54s
U.T.

N74-11616

EXPERIMENTS FOR THE STUDY OF COSMIC GAMMA-RAY BURSTS

T. L. Cline and U. D. Desai
NASA/Goddard Space Flight Center
Greenbelt, Maryland 20771

A Talk Presented at the Los Alamos Conference on Transient Cosmic Gamma- and X-Ray Sources, September 21, 1973, delivered by T. L. Cline.

Several experiments are outlined which are designed for investigating cosmic gamma-ray bursts; they form a research program that includes balloon experiments currently under development and satellite experiments proposed for future missions. The satellite proposals, in most cases, are either suggested for payloads that are presently defined as to experimental complement, or are for hypothetical spacecraft. Thus, these proposals at present serve to indicate, at least, the possible usefulness of various space missions for cosmic gamma-ray burst studies; in the hope that their potential will not be overlooked. Taken as a whole, this program of gamma-ray burst experiments should improve on the present observations of the temporal variations, size spectrum, energy spectra, polarizations, directional locations and distribution of source directions, each by several orders of magnitude of improved resolution or of dynamic range.

I. Detector Development for Extending the Gamma-Ray Temporal Response to Several Nanoseconds

The study of gamma-ray bursts (indeed of most X-ray or gamma-ray astronomical phenomena) has been limited in the past to the use of systems having temporal resolution usually in the fractional-second region, and never better than about 1 millisecond. The potential in short time base astronomy motivated us some time ago, before gamma-ray

bursts were known about, to develop detector systems with fast time response throughout the dynamic range technologically available. Scintillators and photomultipliers limit this to a few nanoseconds. In principle, one could thereby provide as much as a factor of 10^6 improvement in temporal dynamic range. One part of our original motivation came from the suggestion by Colgate that supernovae might produce gamma-ray pulses of duration in the microsecond region; the other part was due to the fact that such techniques had never been developed, and might therefore produce interesting new results or applications for x-ray astronomy. The limiting, few-nanosecond, time resolution is generally outside the capabilities of typical balloon or satellite systems because of the bit-rate limitations on data transmission, which preclude 10^9 Hz linear processing. One way around this limitation is a triggered system with temporary storage; this technique, however, involves preselection of event characteristics. Storage also has a restricted arithmetic limit in dynamic range if it is linear in time scale, and restricted resolution if logarithmic. We are presently developing a balloon gamma-ray detector using an alternative concept, namely, time interval processing.

Figure 1 shows a plot of the differential probability of the occurrence of the succeeding pulse, following any given pulse, on a random basis, given by $dP_o/dAT = \exp(-AT)$. This probability, which in practice is approximated by the corresponding probability per unit time interval on a linear time interval basis, is a maximum for small time intervals.

However, the corresponding probability per unit time interval on a logarithmic time interval scale, $\Delta\pi_o = \exp(-AT_1)-\exp(-AT_2)$, is a power law of index 1 for small times. Thus, the distribution of background pulses, a function that would be a maximum at small times, is converted to one that is a minimum at small times, in order to optimize the pulse-burst signal to background noise ratio. Further, this improvement is enhanced, at the expense of one-half the counting rate, by converting to the probabilities for alternate successive pulses, indicated in the figure by dP_I/dAT and $\Delta\pi_I$. The probability per unit time interval for every alternate pulse, $\Delta\pi_I$, on a log time interval basis, is a power law of index 2 for small times. This sharpens a Poisson distribution to a relatively narrow spike on the logarithmic time interval scale. For a given bit rate, the tradeoff that is accomplished is better ability to resolve fast time fluctuations vs. coarser time histories. Thus, even with a very large scintillator, and with a limited data bit rate, a brief pulse burst consisting of a small number of counts can be separated from the detector background by orders of magnitude if the average time interval between pulses in this burst is significantly less than that of the background. Further, temporal structure in the burst would be indicated by its departure from a random distribution. The electronics required is more involved than for a time-of-flight analyzer, which can measure time intervals to nanosecond accuracy, since the t-o-f system has much more time available to process its information than the time before the next succeeding pulse. The interval analyzer, being deadtimeless, requires more power.

Our first system uses a 25-bin time interval analyzer, ranging from 5 nanoseconds to 0.32 seconds with time interval bins of unity width, i.e. having $(T_2-T_1)/T_1 = 1$. Such a device can be read out several times per second with the modest telemetry requirement of a few kilobits/sec. We hope to balloon-launch soon a simple, omnidirectional detector, using about one square meter of scintillator, with active particle rejection, sensitive to 100-keV to ~1 MeV photons (see Fig. 2a). Plastic, rather than NaI, is used in order to avoid pile-up problems; its efficiency is adequate in this energy range, and energy analysis is not done in this prototype unit. Such a temporal analysis system can be incorporated into any detector with inherently fast response, and, if the balloon trials indicate possible usefulness, variations on this technique will be incorporated in future detector arrangements. Since the cosmic gamma-ray bursts appear to have a wide range of temporal characteristics (with structural elements and even entire burst durations in the <0.1 second region), it should be interesting to explore the possibility that there may be much faster time variations than have been observed.

II. Detector Developments for Extending the Size Spectrum, for Differential Energy vs. Time Studies and Directional Mapping, and for Investigating the Polarization of Gamma-Ray Bursts

Gamma-ray burst studies are presently limited to multiple satellite coincidence techniques in order to obtain a positive identification. Even a single counting rate increase in a collimated telescope does not yet by itself identify an event. An imaging detector which should make it possible to unambiguously identify and study bursts, and which retains a wide-angle sensitivity while incorporating small-angle directional resolution, and is optimum in the pertinent 0.1 to few-MeV range, is the

Compton telescope. This arrangement makes use of two scintillators in coincidence to identify the scattering angle of an incoming photon, relative to the axis of symmetry, but use of the Compton relationship. The inherent susceptibility of such an unshielded system to background, which reduces its potential in conventional or static-source astronomy, may be far less important in the case of gamma-ray burst astronomy because of the relatively high instantaneous flux of gamma-rays encountered from a single direction during an event. Also, quiescent background can be reduced by the use of time-of-flight instrumentation to avoid upwards-moving secondaries. The relative inefficiency of the coincident system is also no great drawback because of the counting rates during the bursts. The use of Compton telescope mosaics can provide greater geometric factor, as well as reducing background by intercomparison or data consistency techniques; it also eliminates the azimuth angle uncertainty inherent in a single, two-element Compton telescope. In addition, it makes possible a polarization study of the gamma rays in a burst by analysis of the azimuth profile of scattered photons. Finally, the scintillators comprising the coincidence system can also be used in the singles mode, with much higher efficiency, to provide high counting rate accuracy on fast time variations.

Thus, an imaging system with wide-angle sensitivity and with directional resolution, fast time structure resolution, differential energy resolution from 0.1 to about 15 MeV, and some polarization capability is possible in a single detector arrangement. This system provides sufficiently unambiguous identification of bursts to be independent of

the need for additional detection by coincident satellites for such purposes as directional mapping studies. A balloon-borne system incorporating all these features is presently being developed (see Fig. 2b). It should not only form the basis of the evolution of a satellite-borne system, but should presently have the capability of extending the knowledge of the size spectrum, energy spectra and anisotropy of gamma-ray bursts from balloon-flight applications, particularly if long-duration exposures can be obtained.

III. An Integrated Satellite Program for Cosmic Gamma-Ray Burst Studies

The most critically important measurement to be performed regarding cosmic gamma-ray bursts is the localization of a source direction to a region only a few seconds of arc in size, so that a source object can be unambiguously identified. The only way this can be accomplished (without data interpretation problems) is a triangulation with deep space vehicles at 1 AU or more distance from each other. In addition, a detailed study of the various properties of the gamma-ray bursts can be investigated with complex payloads on satellites in a far more extensive manner than with balloons. We have therefore proposed that an integrated program of studies be initiated, consisting of these two objectives.

A. Deep-Space Triggers

It was proposed that all satellites capable of carrying a 1 to 2 kilogram apparatus up to distances far from the Earth, and an additional number that orbit the Earth, each include a gamma-ray burst detector. The directional definition capability of such an array is clear: if a burst can be timed to only within 0.1 second, then a 2 AU baseline provides down to 20 arc-seconds accuracy. If the temporal structure

can be observed with sufficient detail to provide 0.01 second timing, then of course $\gtrsim$ 2 arc-seconds resolution will result. At least two deep space triggers (in addition to one near the Earth) are needed to reduce a celestial band of uncertainty to one or two areas of roughly equal uncertainty in declination and right ascension. Further, the statistics of satellite mortality and the variations in launch schedule require that as many instruments be flown as possible in order to maximize the probability of having three detectors sumultaneously sensitive. If the size spectrum has a cutoff near the presently observed number of four or five per year, or if the instruments that are flown are restricted in size, and therefore in sensitivity, such that they cannot respond to smaller and more frequent events, then the requirement of an oversubscription of detectors is even more critical.

The satellites that would be, in principle, available for this purpose include Mariner Jupiter-Saturn, Pioneer-Venus and Helios-B for the deep space missions, and IME, HEAO and various others for the near-Earth missions. Mariner J-S has on board an intense radioactive source in the form of its radioisotope thermal power generator, but estimates show that an appropriate detector could be sensitive to at least the four largest bursts per year. Since this mission flies out to several AU, it is clearly desirable. Pioneer-Venus Orbiter is one deep space mission that does not yet have a selected experiment payload. Since it travels to Venus, it can be at distances of over 1 AU from the Earth. Helios-B will have an elliptical orbit with a perihelion of about 0.3 AU and an aphelion of 1 AU, so that it can be at distances from the Earth of up to 2 AU. Each of these should certainly carry a gamma-ray burst

detector.

Near-Earth missions include IME-Heliocentric and the various Earth orbiters, such as IME-Mother, HEAO, and a variety of satellites having prime objectives other than interplanetary studies or astrophysics. As many of these that can be incorporated should be. Most, if not all, of the detectors will have to include a considerable amount of data storage, in addition to the electronic intelligence which is needed to recognize a candidate event, since the bit rates available will be only in the 1 to several/second range. We have proposed that a standard trigger be developed which could be duplicated and adjusted to the telemetries of all these spacecraft, so that the costs of the endeavor be minimized. It still may be possible to have these detectors included on a variety of the contemplated vehicles, since their assumed launch dates range from about 2 or more years from now for Helios-B to at least four years from now for the others.

B. Large Gamma-Ray Burst Payloads

We have proposed that a large payload for the detailed study of gamma ray bursts, in addition to the small trigger payloads, be flown on a satellite in the near future. This could be accomplished by using an Explorer-type mission, or with a $\approx$ 100-lb. addition to the HEAO X- and gamma-ray satellite. The scientific justification for a significant effort is clear, but whether an entire Explorer mission can be dedicated to this purpose in the very near future, or whether a HEAO can be adjusted to accommodate an extra payload, is unknown at present. We proposed that such a payload should have at least two separate experiments, in order that a variety of measurements can be made.

The primary objectives of a gamma-ray burst payload should include i) a detailed energy vs. time study, in which frequent differential energy spectra are determined as a function of time throughout each burst history, ii) a rapid time study, in which very fast components can be detected on a time basis too fine for complete energy analysis, and iii) a directional mapping study, for the determination of the anisotropy of source direction as a function of burst size.

First, energy spectra need to be studied in greater detail than is presently possible, not only to search for monoenergetic lines, detection of which would go a long way towards identifying some of the basic processes involved, but also to study the evolution of the burst continuum energy spectrum. Detailed spectra should help in critical evaluation of theoretical models if resolution is available that is sufficient to map out whether, for example, a time-varying blackbody spectrum exists or if a recognizable secondary process exists, such as time-varying thermal bremsstrahlung. Since the pulses exhibit a very fast time history, the temporal resolution of individual spectra will have to be quite good, perhaps on the millisecond scale. In order to get sufficient statistics to have well-defined differential energy spectra on these short time scales, detectors that are considerably larger than those presently used will be required. In order to avoid instantaneous pulse pile up that may occur in large, single detectors, either NaI mosaics with individual readouts or plastic scintillators and/or solid state detectors, which have orders of magnitude faster pulse response, will be needed.

Second, time variation studies are desired on a scale even faster

than can be accommodated with energy analysis. It may be that more than one process has been detected by the Los Alamos observations, since some of their events have multiple pulse structure that goes on for tens of seconds, while others are completely finished in a fraction of a second. The assumption that all gamma ray bursts are due to some single source process is the simplest at this point, but the data suggest that fine time resolution studies may show that at least two separate categories of events can be clearly defined. If such is the case, they may actually originate in two different source populations. Time resolution in the microsecond to millisecond region will be needed to fully investigate the properties of events like those few very fast (< 0.1 second) cases discussed by the Los Alamos authors. For this reason, we feel that both extremely fast time studies and moderately fast time vs. energy studies are needed in the next generation of detectors.

Third, the mapping of source directions is an objective quite apart from source identification. Triangulation from deep space vehicles may localize a few sources to arc-seconds of accuracy, but observations of the approximate source directions of the dozens to hundreds of other events that may be observed with detectors somewhat more sensitive than the trigger detectors will provide much better statistics as to directional mapping and the anisotropy as a function of burst size. This measurement could be made by flying an imaging device, such as a Compton mosaic, on a small satellite. The results of this observation should be important in terms of determining the source distribution in star clusters, spiral arms, galactic groups, clusters, or whatever. We feel that this is one of the parameters that should be investigated in the next gener-

ation of experiments, particularly if the gamma-ray bursts turn out to be composed of two or more populations or categories of events.

Finally, it is contended that omnidirectional detectors, or mosaics of wide angle detectors, are better for all these purposes than collimated telescopes, because of the relative sensitivity. Obviously, if a telescope can view only 10^{-3} of the sky at a time, its usefulness will be negligible if the size spectrum turns out to have a real cutoff such that there exist only a dozen or so visible events per year. Its usefulness, relative to that of the systems we have proposed, would also be extremely limited even if the size spectrum does have an indefinite extent, if its sensitivity to the more frequent, smaller events is severely limited by counting rate statistics.

Figure Captions

Fig. 1. A plot of differential probabilities, dP/dAT, and probabilities per unit time interval, $\Delta\pi$, for succeeding events (subscript o) and for alternate events (subscript I) which comprise a Poisson distribution, plotted on a logarithmic time interval scale.

Fig. 2a. A large area, single-scintillator gamma ray detector for a balloon-borne search for fast time variations, to incorporate a logarithmic time interval analyzer. Charged particles are vetoed both on a pulse-height basis from the large scintillator itself, and on a coincidence basis from the thin cover scintillator.

Fig. 2b. A compton mosaic gamma ray detector, in which a coincidence between the top and bottom arrays initiates energy and time analysis of the input pulses. Each photon producing a coincidence between any given upper and one such lower scintillator provides an possible zenith angle; scatter diagrams of all such coincident photons produce a mean angle for that coincident element; all such coincidences between a different set of scintillators produce another mean scattering angle about the other telescope axis; the intersection of these yields candidate azimuth angles. Thus, unambiguous source directions can be determined if a sufficient number of photons are analyzed. A polarization would be apparent in an asymmetric distribution of azimuthal scattering.

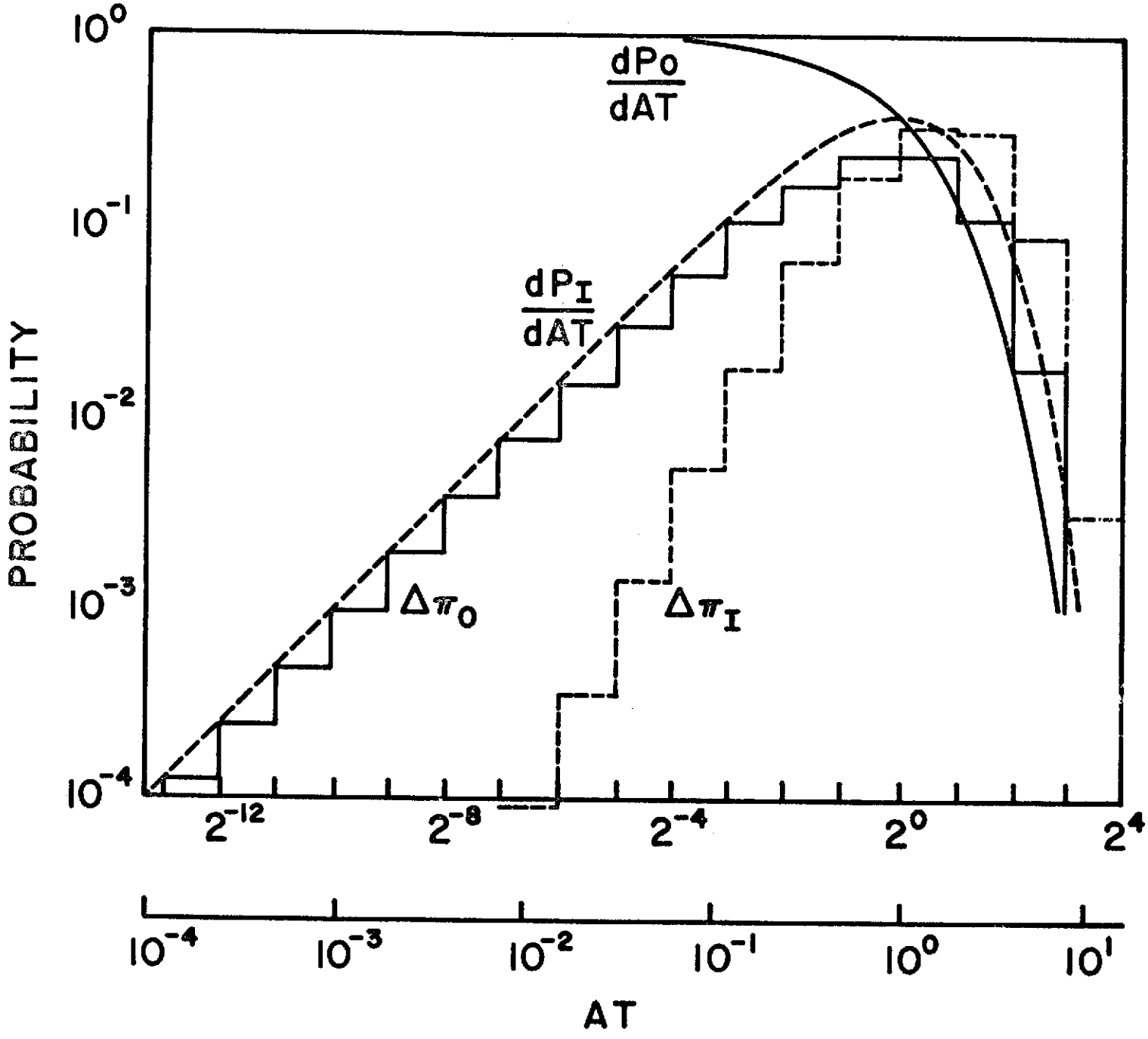
PROBABILITY
10^{0}
10^{-1}
10^{-2}
10^{-3}
10^{-4}
$\frac{dP_O}{dAT}$
$\frac{dP_I}{dAT}$
$\Delta\pi_O$
$\Delta\pi_I$
2^{-12}
2^{-8}
2^{-4}
2^{0}
2^{4}
10^{-4}
10^{-3}
10^{-2}
10^{-1}
10^{0}
10^{1}
AT

42-INCH DISK
>50 keV
5nS
>1 MeV
5nS
>0.1 MeV
2nS
ANTI
COINC
T.I.A.
θ_1
θ_2
e_1
e_2
γ_1
γ_2
ANY UPPER
ANY LOWER
COINC
GATE
PHA
PHA
PHA
TIME